NAVAL POSTGRADUATE SCHOOL

MONTEREY, CALIFORNIA

THESIS

HYBRID INSPIRED TRIBOELECTRIC NANOGENERATOR USING CONTACT SEPARATION MODE

by

John M. Barmann

June 2021

Thesis Advisor: Young W. Kwon
Co-Advisor: Jarema M. Didoszak

THIS PAGE INTENTIONALLY LEFT BLANK

REPORT DOCUMENTATION PAGE			Form Approved OMB No. 0704-0188

1. AGENCY USE ONLY *(Leave blank)*	2. REPORT DATE June 2021	3. REPORT TYPE AND DATES COVERED Master's thesis

4. TITLE AND SUBTITLE HYBRID INSPIRED TRIBOELECTRIC NANOGENERATOR USING CONTACT SEPARATION MODE	5. FUNDING NUMBERS
6. AUTHOR(S) John M. Barmann	
7. PERFORMING ORGANIZATION NAME(S) AND ADDRESS(ES) Naval Postgraduate School Monterey, CA 93943-5000	8. PERFORMING ORGANIZATION REPORT NUMBER
9. SPONSORING / MONITORING AGENCY NAME(S) AND ADDRESS(ES) N/A	10. SPONSORING / MONITORING AGENCY REPORT NUMBER

11. SUPPLEMENTARY NOTES The views expressed in this thesis are those of the author and do not reflect the official policy or position of the Department of Defense or the U.S. Government.

12a. DISTRIBUTION / AVAILABILITY STATEMENT Approved for public release. Distribution is unlimited.	12b. DISTRIBUTION CODE A

13. ABSTRACT (maximum 200 words)

The triboelectric nanogenerator (TENG) concept was used to build four contact separation TENG models to harvest mechanical vibration from an aircraft wing on an unmanned air and surface vehicle. The first three models used a hexagonal base structure with cylindrical pegs and solid rectangular bar on top. The last design used a rectangular box structure with a free moving bar to convert mechanical vibration output into electrical power. To simulate the vibrational motion of an unmanned aerial vehicle wing, a linear arm motor was used at various speeds to test each model for harvesting mechanical motion. The experimental results showed that the model that produced the maximum voltage was the attached solid bar design. The free bar structure design allowed the use of two electrodes in one structure. The ability to use two electrodes for one model enhanced the electrical power production. The finite element method analysis showed that the rectangular bar models would produce the best electrical output based on their contact frequency, matching with the experimental results. In conclusion, the results showed that the two rectangular bar TENG models can harvest mechanical vibrational energy and convert it into electrical power. Further research into using additional free bar TENG models together in series would demonstrate the ability to harvest additional voltage to store and use for sensor power.

14. SUBJECT TERMS triboelectric generator, peizoelectric generator, triboelectric nanogenerator, TENG	15. NUMBER OF PAGES 77
	16. PRICE CODE

17. SECURITY CLASSIFICATION OF REPORT	18. SECURITY CLASSIFICATION OF THIS PAGE	19. SECURITY CLASSIFICATION OF ABSTRACT	20. LIMITATION OF ABSTRACT
Unclassified	Unclassified	Unclassified	UU

NSN 7540-01-280-5500 Standard Form 298 (Rev. 2-89) Prescribed by ANSI Std. 239-18

THIS PAGE INTENTIONALLY LEFT BLANK

Approved for public release. Distribution is unlimited.

HYBRID INSPIRED TRIBOELECTRIC NANOGENERATOR USING CONTACT SEPARATION MODE

John M. Barmann
Lieutenant, United States Navy
BS, Northern Illinois University, 2013

Submitted in partial fulfillment of the
requirements for the degree of

MASTER OF SCIENCE IN MECHANICAL ENGINEERING

from the

NAVAL POSTGRADUATE SCHOOL
June 2021

Approved by: Young W. Kwon
Advisor

Jarema M. Didoszak
Co-Advisor

Garth V. Hobson
Chair, Department of Mechanical and Aerospace Engineering

THIS PAGE INTENTIONALLY LEFT BLANK

ABSTRACT

The triboelectric nanogenerator (TENG) concept was used to build four contact separation TENG models to harvest mechanical vibration from an aircraft wing on an unmanned air and surface vehicle. The first three models used a hexagonal base structure with cylindrical pegs and solid rectangular bar on top. The last design used a rectangular box structure with a free moving bar to convert mechanical vibration output into electrical power. To simulate the vibrational motion of an unmanned aerial vehicle wing, a linear arm motor was used at various speeds to test each model for harvesting mechanical motion. The experimental results showed that the model that produced the maximum voltage was the attached solid bar design. The free bar structure design allowed the use of two electrodes in one structure. The ability to use two electrodes for one model enhanced the electrical power production. The finite element method analysis showed that the rectangular bar models would produce the best electrical output based on their contact frequency, matching with the experimental results. In conclusion, the results showed that the two rectangular bar TENG models can harvest mechanical vibrational energy and convert it into electrical power. Further research into using additional free bar TENG models together in series would demonstrate the ability to harvest additional voltage to store and use for sensor power.

THIS PAGE INTENTIONALLY LEFT BLANK

TABLE OF CONTENTS

LIST OF FIGURES

LIST OF TABLES

THIS PAGE INTENTIONALLY LEFT BLANK

LIST OF ACRONYMS AND ABBREVIATIONS

BS-TENG	Ball Sphere TENG
FEM	Finite Element Method
LED	Light Emitting Diode
MAX	Maximum
MIN	Minimum
PTFE	Polytetrafluoroethylene
RPM	Revolution Per Minute
TENG	Triboelectric Nanogenerator
UAV	Unmanned Aerial Vehicle
V	Voltage

THIS PAGE INTENTIONALLY LEFT BLANK

ACKNOWLEDGMENTS

I would like to thank Professor Kwon for his constant support and help throughout my time at NPS, especially working on my thesis. I would also like to thank Professor Jarema Didoszak for his support on my thesis work and LT June Capelle for his help in getting my thesis started. Finally, I would like to thank my wife who supports me and my family every day; without her, I would not be here today.

THIS PAGE INTENTIONALLY LEFT BLANK

I. INTRODUCTION

Harvesting natural energy such as wind and wave motion is a proven method to power various mechanical and electrical machines, from small scale sensors to large hydroelectric plants. Vibrational energy is a common form of energy found in everyday life. Harvesting vibrational energy helps change the way unmanned ships and aircrafts are designed when vibrational energy is a main power source. One way to harvest vibrational energy is to use a device that takes mechanical motion of the vibration and translates it into electrical output. The triboelectric nanogenerator (TENG) has proven to be leading source in harvesting natural energy such as wind, wave motion, and vibration, converting mechanical input to electrical output.

A. TENG OVERVIEW

A TENG uses the triboelectric effect where two dissimilar materials contact one another where electrostatic charges from one material transfer to the other on the surface. As the contact between the materials continues the triboelectric charges collect and then promote transfer of electrons through the electrode to provide electrical output to the circuit. The triboelectric charges are a driving force for electrons to flow and balance the electric potential drop created [1]. The material that can be used to create the triboelectric effect is any material that attracts a charge; but the primary uses of polytetrafluoroethylene (PTFE) and silicone are best for obtaining a negative charge while nylon and metal are best for positive charges. Together, the PTFE and nylon or metal make up the material needed for a TENG to sufficiently produce electrostatic charges [2].

The fundamental theory behind the TENG is derived from Maxwell's displacement current [3]. The equation is defined below:

$$J_D = \frac{\partial \boldsymbol{D}}{\partial t} = \varepsilon \frac{\partial \boldsymbol{E}}{\partial t} + \frac{\partial \boldsymbol{P}_S}{\partial t} \tag{1}$$

where D is the displacement field, ε is the permittivity of the medium, E is the electric field, and P_s is the polarization due to the surface polarization charges from either piezoelectric or triboelectric effect [2]. As the TENG device operates, by some mechanical mechanism, an electrostatic charge occurs and the triboelectrification grows between the two materials as they continuously contact each other. This is the basis for the general model of a TENG.

Wang et al. [2]. found that there are four basic concepts for designing a TENG; they are vertical contact-separation, contact-sliding, single-electrode, and freestanding triboelectric-layer modes. Each mode can harness a mechanical output; some modes are best suited for specific outputs. A further literature review of each mode will be made to best assess which one is suited for harnessing the vibrational energy of an aircraft's wing and the vibrational motion of a wave impacting on the hull of a vessel transiting through the water.

B. RESEARCH OBJECTIVE

The objective of this research is to find a suitable solution to harnessing the vibrational energy generated from air flowing over the wings of an UAV and the impact of waves on a USV's hull as it transits through the water. This vibrational energy can be considered renewable energy that is left unharnessed. A TENG device can be developed to harvest the vibration motion converting it to an electrical output. The designed TENG can be incorporated into the structure of either UAV or USV to harness the vibrational motion. Before incorporating the design into the structure of the vehicle the designs must be able to harvest the vibrational motion. Four design iterations were made that enabled harvested the vibrational motion. This study will simulate the vibrational motion using two methods. First method will be a manual excitation to ensure the designs are capable in producing voltage. The second method is using a linear arm motor at various speeds. The basis for the TENG device will use contact separation mode with two pieces of dissimilar materials, copper, and PTFE tape, which are applied to 3-D printed structures. Additionally, the density and stiffness for the designs will be analyzed using finite element method (FEM) to determine how the contact separation changes with different design parameters.

II. LITERATURE REVIEW

The triboelectric effect occurs so frequently in everyday uses that it goes unharnessed and unused. The first development of a TENG was established by Wang et al. [2]. in 2012 where the harvesting of mechanical output energy was done utilizing the triboelectric effect between the two materials. The utilization of the triboelectric effect along with electrification induction showed that there is a way to harness these energies and power sensors and systems at low frequencies with very little power needed [2]. The overall cost of producing a TENG is very low, and the material needed is easily found or produced at a low cost. They can be light weight and small in scale so that incorporating it into a system does not interfere with its' primary function.

One of the first TENG designs conceived was the contact-separation mode specifically the vertical contact separation, shown in Figure 1. This mode consists of two electrodes that are connected to an external load and two dielectrics for contact electrification. Due to the contact electrification the two contact surfaces are positively and negatively charged and as the continuous contact builds an electrification field occurs that drives electrons through the external load [2].

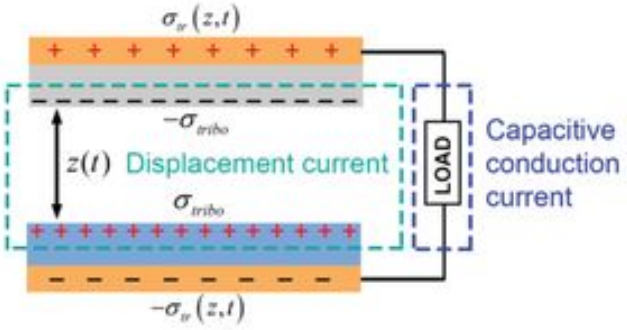

Figure 1. Vertical contact separation TENG. Source: [2].

As seen in Figure 2, the triboelectric nanogenerator shows that the two electrodes create positive and negative charges on the surface through the triboelectric electricity, which is independent of the displacement current. With increase in contact cycles, there is

an accumulation of electrons that then build an electric field which drives the transfer of electrons through the load. This electron transfer is a function of the displacement current that takes mechanical energy into electricity [3].

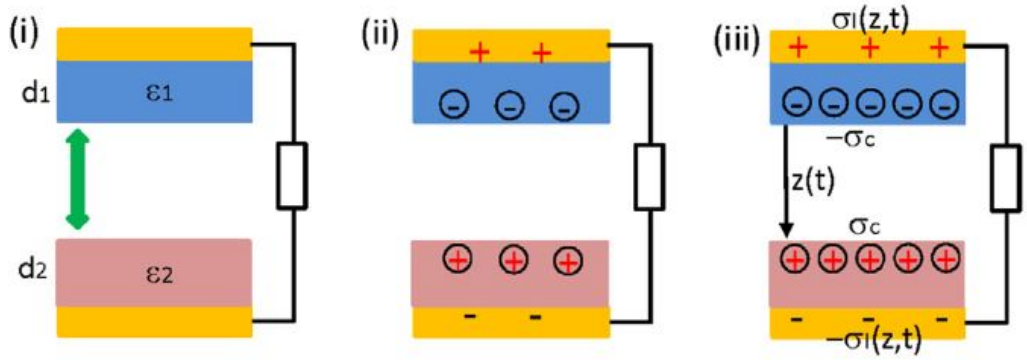

Figure 2. Triboelectric nanogenerator using contact separation technique. Source: [3].

The first mode is the basis for how the triboelectric nanogenerator operates in producing electricity. Three different modes can be derived from this concept using a variation of the triboelectrification effect. The other three modes are lateral sliding, single-electrode, and freestanding, which are shown in Figure 3.

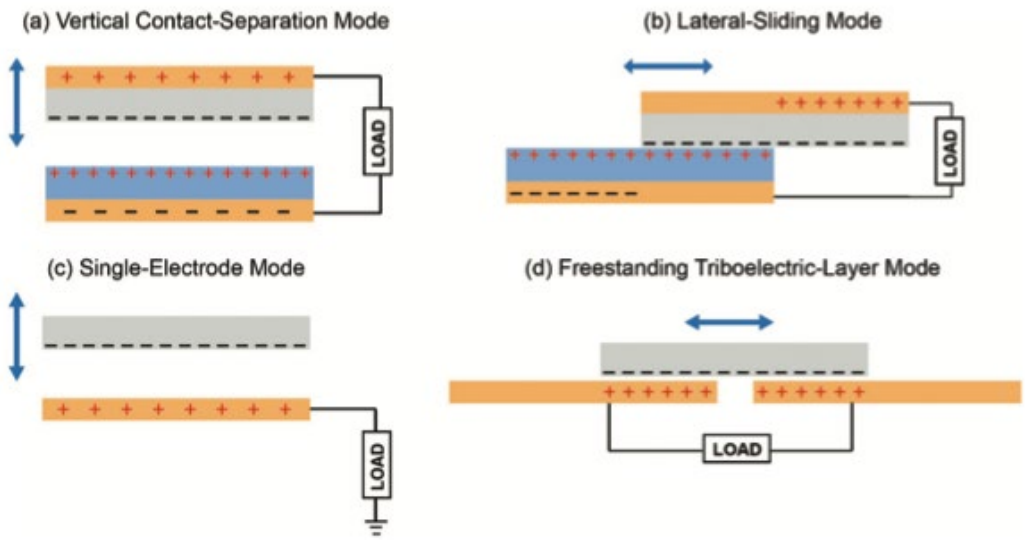

Figure 3. Four triboelectric nanogenerator modes made for transferring mechanical energy to electricity. Source: [2].

The lateral sliding mode uses two materials that are contacting each other directly while undergoing a lateral motion. The lateral movement of the two electrodes generates positive and negative charges along their surfaces. As they move laterally, there is an uneven balance of electrons on either surface which accumulate over time building the electric field. The electric field then drives the electrons through the external load. The displacement current is in the parallel direction of the lateral movement, like the vertical separation mode. The lateral sliding can be operated through rolling interface of two materials as well as the sliding effect [2,3].

The single-electrode mode uses the ground as the electrode with no need for the use of electric conductor. This means that the energy harvested can be done through a metal material and the ground itself as the electrode [2,3]. The free-standing triboelectric layer model allows for no grounding to be needed. Instead, there are two symmetric electrodes with a free moving object that creates the triboelectric effect. The free-standing mode allows for harvesting energy provided that the asymmetric material is charged previously. The four modes primarily show the theory of the triboelectric effect and its applicability in harnessing mechanical energy. The modes can be made to work together or on their own to harness the energy depending on situation.

Various types of energy have been harvested in the past to convert the mechanical energy into electricity. To harness wave energy the contact and sliding mode TENG was found to produce electricity capable of powering sensors or even charging capacitors. Xu et al. [5]. used a combination of triboelectric effect and electrostatic effect to harness the water wave energy by implementing a Ball sphere TENG (BS-TENG) structure (Figure 4). The BS-TENG structure consists of two metal electrodes on the outer portion of the sphere and a coated dielectric surface on the inner part of the sphere, depicted as the grey surface in Figure 4. The ball is made from silicone rubber with a UV treatment applied to it to soften the material giving a true surface area contact when excited by the wave motion.

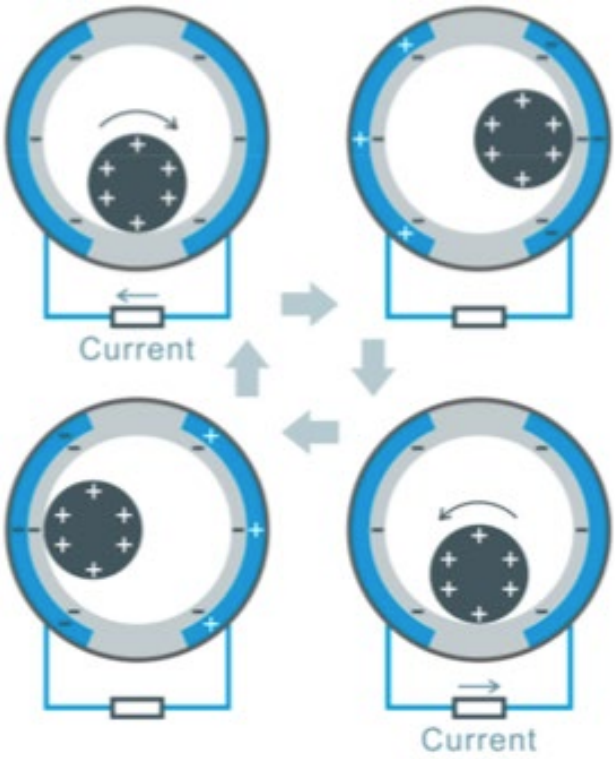

Figure 4. Ball sphere TENG structure used to harness water wave energy.
Source: [5].

The BS-TENG was applied in a single unit format and then tried together with multiple units connected by three different types of materials, string, elastic strip, and a rigid plate. Each connection was tested to find the amount of charge and current capabilities

when connected as an entire unit. Figure 5 shows that the output for the entire system produced more voltage when linked together than as a free-standing unit. The free-standing unit produced current that was lower than the linked model. Due to the orientation of the free-standing model, it was not always in the proper position, so the amount of voltage produced decrease due to the missed contact surface of the unit.

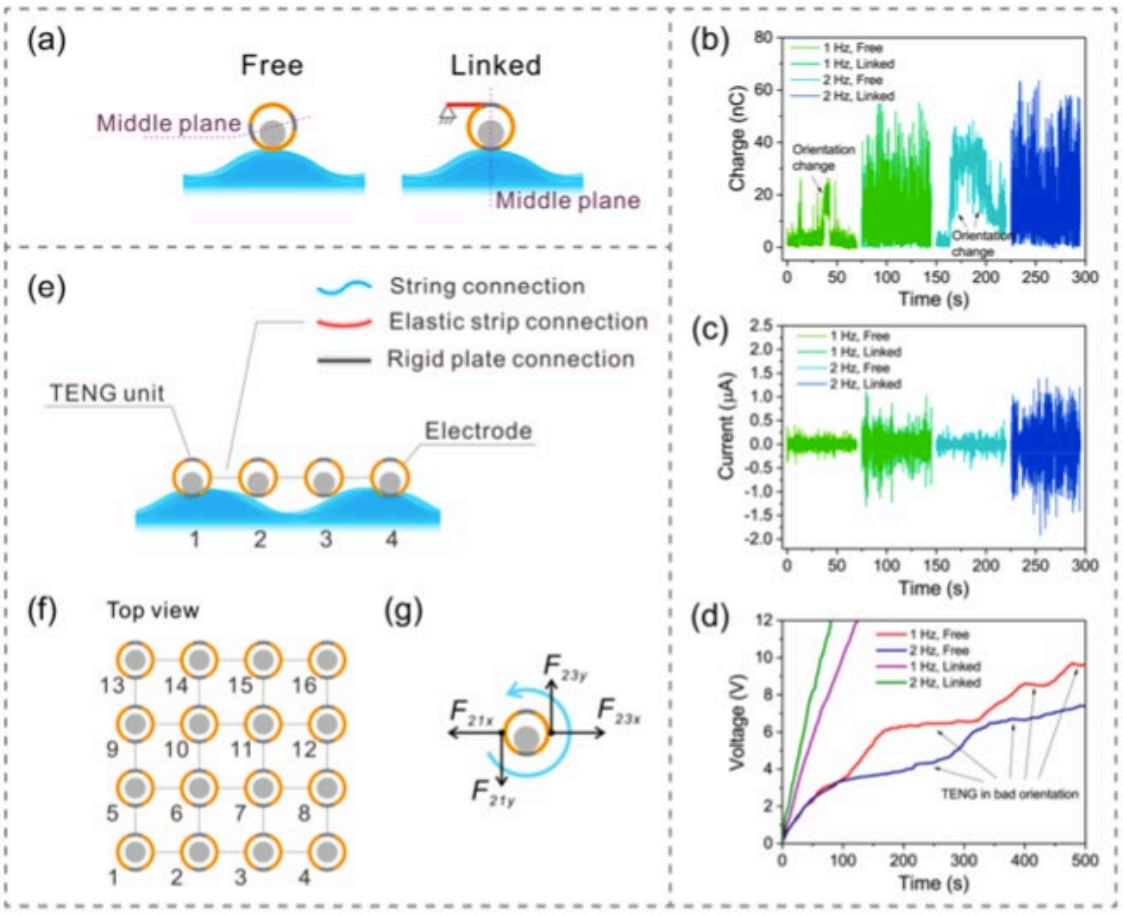

Figure 5. BS-TENG design description and results; (a) BS-TENG used with free connection and linked connections, (b)-(d) show the charge, current and voltage capacity for the unit, (f) shows the total number of units for the entire system, (g) shows the directional forces for an individual unit based on wave motion. Source: [5].

This study showed that to harness water wave motion the free-standing unit must have the correct orientation to maximize the use of the contact surface area of the metal

electrode and dielectric material of the inner surface. This design helps establish the use of both the triboelectric effect and the electrostatic induction as one model.

Water wave motion is just one of the many forms of energy found in everyday life that can be harvested. Another motion is vibrational motion. One aspect of vibrational motion was found with operation of a motor that caused residual vibration motion. Xiu et al. [6]. found that a basic honeycomb structure design can have an ideal use for a TENG to harvest the residual vibration (Figure 6).

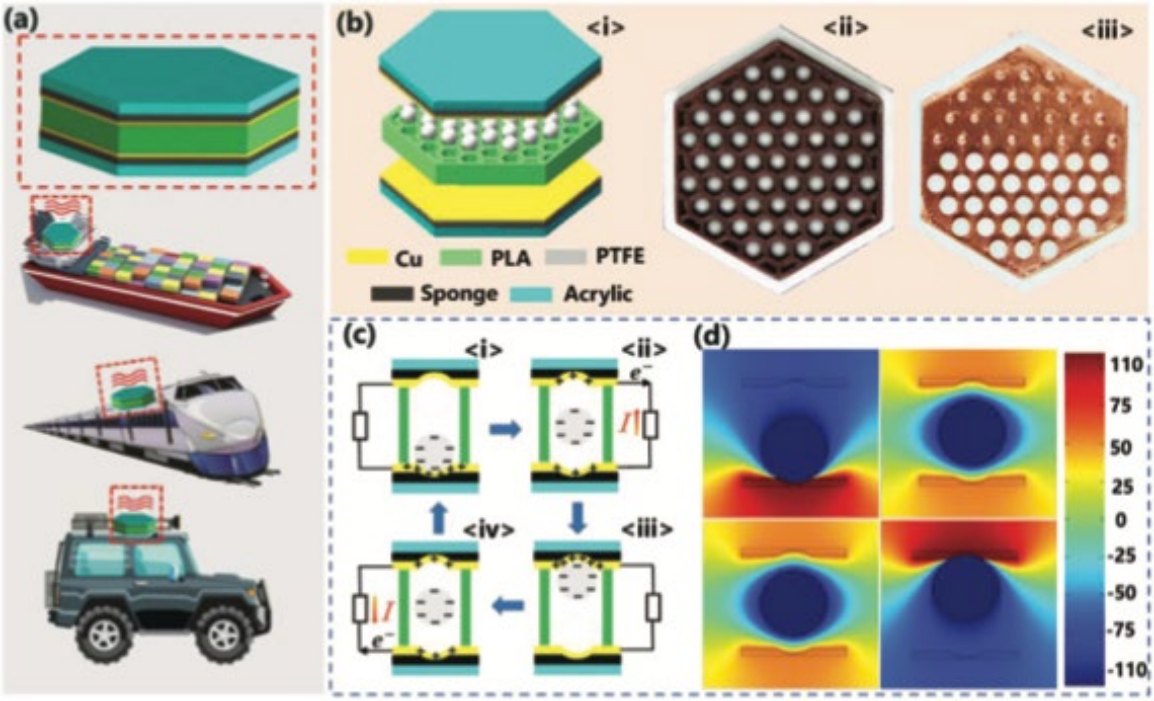

Figure 6. HIS-TENG design description; (a) The encased HSI-TENG showing the possible uses for the design, (b) The design overlay for each layered part of the design and the PTFE balls placed in the honeycomb structure with the copper sheet, (c) The displacement of the PTFE balls with the degree of contact when in motion. Source: [6].

The small size of the honeycomb structure would be able to have less spacing than a square grid structure when using PTFE balls as the excitation material. (Figure 7). The PTFE balls had a diameter of 5mm, the amount of spacing for each cell was reduced when

using the hexagonal shape versus the square where more unused spacing was present. Additionally, the hexagonal shape allowed more freedom of movement for the balls leading to a more efficient motion when harvesting the vibration energy. The second material used to induce a triboelectric and static induction was copper platting on the top and bottom of the structure. The balls are placed in the honeycomb slots and when excited from vibrational motion, they would separate from the bottom and be in continuous motion between the two copper surfaces. The results of the experiment showed a bandgap between the vibrational amplitude and the vibrational acceleration. For the PTFE ball to separate from the bottom electrode layer a displacement criterion needed to be obtained that exceeded the bandgap.

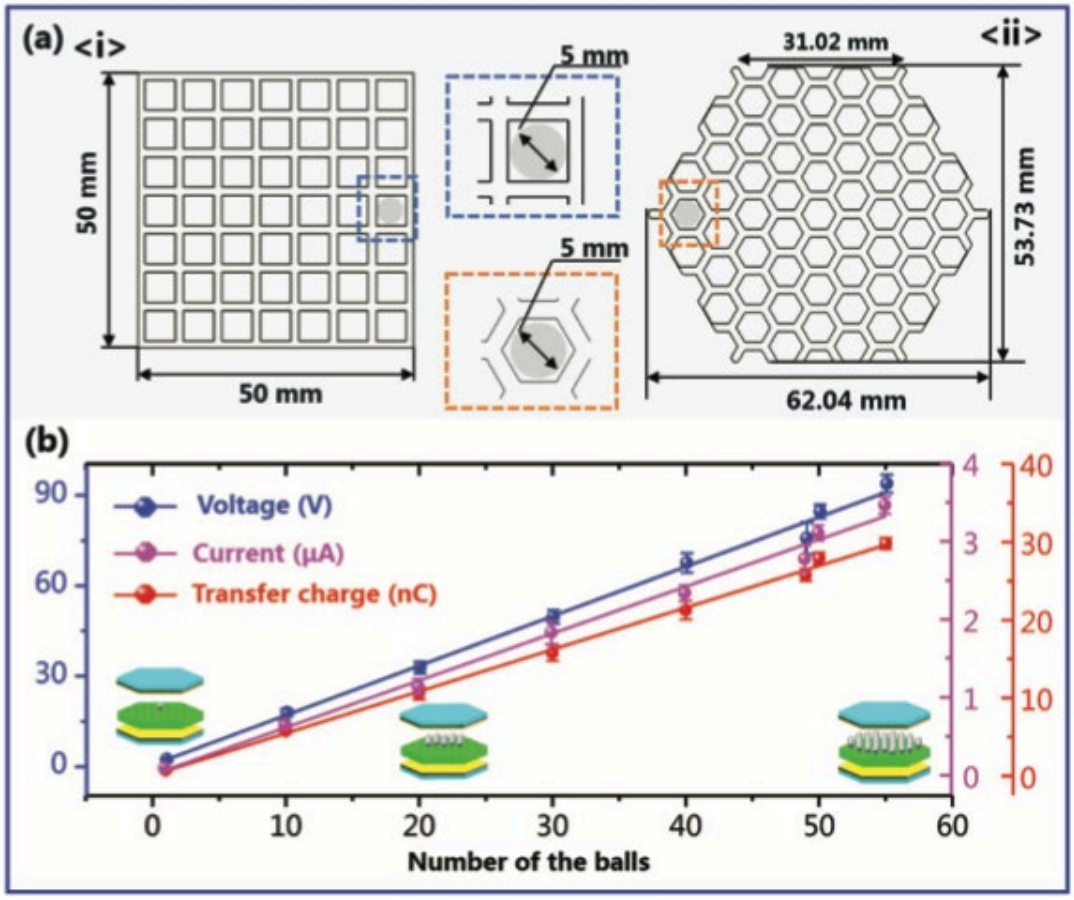

Figure 7. HIS-TENG honeycomb structure design; (a) The honeycomb structure dimensions and the comparative to square grid dimensions, (b) the voltage produced per the number of PTFE balls used in the design. Source: [6].

An increase in the number of PTFE balls used for the design showed an increase in both current and voltage. As the more PTFE balls are used the amount of charge transferred increased. This design improved upon the use of the triboelectric effect in harvesting vibrational energy of a moving machinery/motor.

The described design by Xiu et al. [6]. showed that using the compact structure of a hexagonal honeycomb shape the use of multiple electrodes produced a steady state of electricity. The hexagon shape was used as the base of my TENG design for my thesis incorporating the contact separation of either fixed or free electrodes such as a rectangular bar or cylindrical pegs.

III. DESIGN DESCRIPTION

To harvest the vibrational and wave motion energy, a new design was developed as a multifunctional sandwich structure. This new design will be designed so that it can be put into a UAV wing structure. To account for the wing structure the design will have three parts to make up a sandwich structure. The structure consisted of three 3-D printed parts: a top, middle, and bottom section. The bottom of the structure had three variations: first, a row of six attached cylindrical pegs, the second, a row of six free standing cylindrical pegs, and third an attached single horizontal bar. The Teflon tape was applied to the cylindrical pegs for the first two designs and the bar for the third design. The middle section acted as the free moving piece with four slotted ellipticals where the inner most two are covered with copper tape. The cylindrical pegs and bar were placed in either the inner most two slots to create the triboelectric effect between the copper and Teflon surfaces. The total surface area of the copper tape section was 484.866 mm^2 for one side as depicted in Figure 8. The final part of the structure was the top, which was formatted for each design to hold either the cylindrical pegs or the rectangular bar.

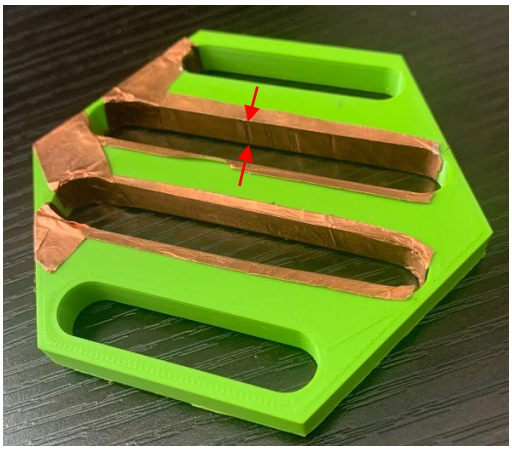

Figure 8. Middle section with copper tape.

The constant peg design had a stable structure when all three parts were together. The stability of the structure allowed the second piece to move freely, contacting the

cylindrical pegs evenly. Each cylindrical peg had a radius of 2.74 mm and a length of 23 mm giving a total lateral surface area of 395.966 mm^2. The amount of surface area that contacts the copper tape is 3.2 mm^2 for each peg, with a total of 19.2 mm^2. When in motion the cylindrical pegs were only contacting 4% of the total surface area available leaving a large amount of area unused.

The free pegs design was unstable as it underwent motion. The top of the structure does not hold the cylinders in place which caused multiple cylinders to fall out of the holder. Additionally, as the slotted middle section moved, the cylinders become dislodged. To prevent this, the middle section needed to be stable so that only the cylinders moved. The freedom of the cylindrical pegs showed a possible cancellation effect occurring. As one cylinder contacts the copper tape another will contact the other side cancelling the gained charge resulting in no net charge transferred. Another flaw in the design is the lack of stability of the structure that prevented the cylinders from maintaining their position in the holder. The surface area of the pegs was the same as the constant peg design.

The single bar design was stable and created a sandwich structure. The total surface area for the bar is 756.768 mm^2, and the bar should contact the entire surface area of the copper tape. The surface area of the tape accounts for 64% of the bar's surface area. Being able to contact the entire surface area of the copper tape, the output voltage should exceed the previous two designs.

When put the structure was put together the bar and copper surface show spacing between the two, as shown in Figure 9. The uneven contact could be caused by the 3-D printing of the bar. At the bottom of the bar minor defects are present which protrude outward. These defects can prevent contact between the two surfaces. The gaps found would prevent proper transfer of charges leading to lower voltage generated.

Figure 9. Gaps between copper tape and bar.

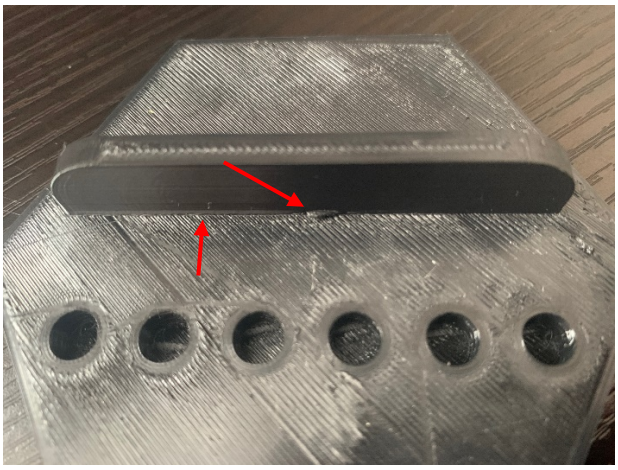

Figure 10. Defects at the bottom of the bar.

A fourth design was used to optimize the single bar design, using a square structure instead of a hexagon shaped structure. Using a square structure could improve the contact of the Teflon and copper surfaces. Furthermore, the square structure could improve the 3-D printing of the design, using less material and a simpler design that produces less defects. Allowing the bar to move freely, like design #2, would potentially give a more varied approach to harnessing the vibration energy. Design #4 consists of three parts, two bar holders and a rectangular bar as shown in Figure 11.

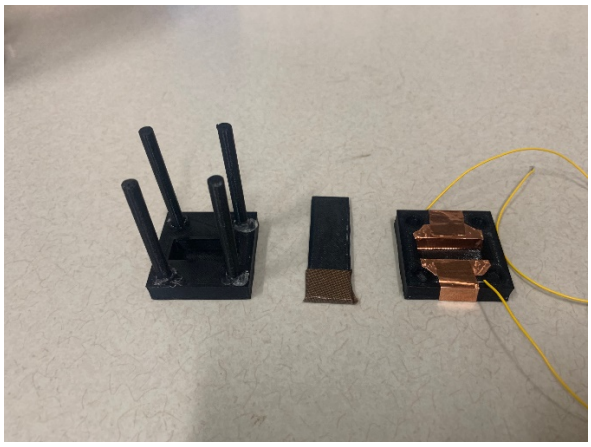

Figure 11. Design #4, free bar excitation mode with three parts. Two bar holders and free rectangular bar.

The amount of contact available for the PTFE on the rectangular bar is 5mm on the top and bottom, shown in Figure 12. The holder has dimension of 35 X 35 X 6mm with a middle cut that has a depth of 6mm. The cut is where the bar will be placed to contact the copper tape, as depicted in Figure 13. This design allows the use of both sides of the rectangular bar where either holder can have copper tape and wiring to harness the vibration energy. One problem with design #3 was the printing of the solid bar to the base structure where defects were found. These defects led to minor gaps between the PTFE and the copper tape, not allowing proper contact between the two surfaces. In design #4, there were no defects found in either the bar itself or the holder allowing for even contact between PTFE and copper tape surfaces. The total surface area of the PTFE on the rectangular bar is 75mm^2 for either the top or bottom. The copper tape on the bar holder has a surface area of 125mm^2. When full contact is made between the structures there is 50mm^2 not used. Each of the designs will undergo the same experiments to determine which design harvests vibrational energy the best.

Figure 12. Rectangular bar with PTFE tape showing 5mm contact spacing at the tip.

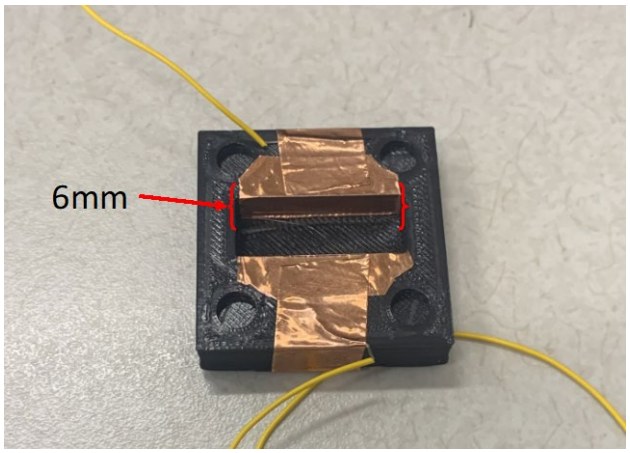

Figure 13. Rectangular bar holder with copper tape and wiring around the middle cut. Dimensions of the middle cut are 25 X 6 X 10mm.

Table 1. Design pros and cons for the four TENG models.

Design	Pros	Cons
Attached Pegs 	One solid structure with three pieces. It has multiple rows of pegs to use as electrode layer to enhance voltage production.	It has a small contact surface area which leads to lower voltage output.
Free Pegs 	Freedom of movement for each peg allows for more contact to occur between copper and Teflon tapes.	Low voltage output Unstable structure Cancellation of electrons between the two surfaces due to multiple pegs moving at same time. Smaller contact surface area, lower voltage output.
Single Bar 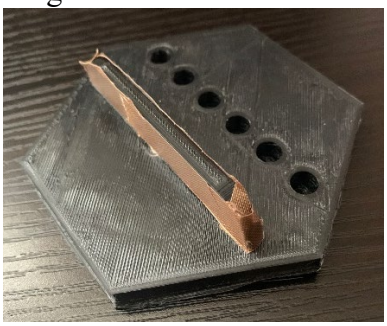	One solid and stable structure. The contact surface has a larger surface area than the cylindrical pegs which increasing voltage production.	Only one electrode leading to a lower voltage production. Defects on bar from 3D printing cause uneven contact between Teflon and copper tapes.
Free Bar 	Stable and solid structure. Able to use two sides of the free bar for two electrodes that increases voltage production. The rectangular bar is free to move for increase surface contact.	Smaller than the previous three models. Smaller contact surface area causes less voltage produced for one unit.

IV. DESIGN EXPERIMENTS

Two experiments were used to test each TENG design, a manual excitation, and a linear motion excitation. The manual excitation was used as a base line for voltage production. The second experiment used linear motion excitation through a linear arm motor gear box with four different speed variations. This allowed for a more controlled excitation and better understanding for how much voltage can be produced. The initial hypothesis is that at the range of 60–100RPM the designs would produce voltage as this is the typical range of RPM undergoing from vibration of wind over an airwing of a UAV or wave motion on the hull of a USV.

A. MANUAL EXCITATION EXPERIMENT

To establish the design effectiveness, manual excitation by hand was done to each design. The designs were handheld and underwent as close as possibly the same motion to simulate vibration of aircraft wing or wave vibration against a ship's hull. The experiment lent to a bias because of the random motion generated by hand cannot be duplicated to the exact motion for each design. It is hard to measure what motion was being done to each device to make a full comparison, so a consistent time interval was chosen at 5s. First each design was tested on its own in series with the oscilloscope. Then, each design was connected in series to a rectifier through a circuit board to enhance any voltage produced and the voltage was measured through the oscilloscope. The constant peg TENG is shown in Figures 14 as an example for the experimental setup used on the designs.

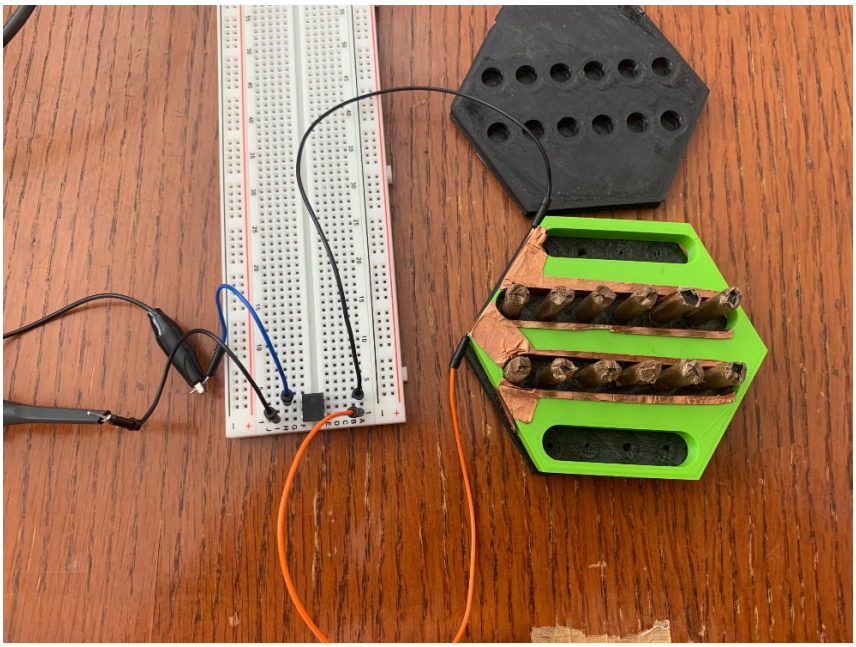

Figure 14. Constant peg TENG design setup for manual excitation experiment with rectifier and oscilloscope in series.

B. LINEAR MOTION EXPERIMENT

To establish a consistent motion output, the linear motion arm was used to excite the different design models simulating the vibration motion. The linear motion arm was previously used by Mann [7] in her thesis to study wave motion energy harnessing. The device used has a maximum 350 RPM when at full speed. The three designs that produced the most voltage under manual excitation were tested under this linear motion with four different speeds, 1/3,1/2,2/3, and full speeds. For each speed, the voltage produced was measured using an oscilloscope wired in series with a rectifier to convert the AC produced current to DC output (Figure 15–17).

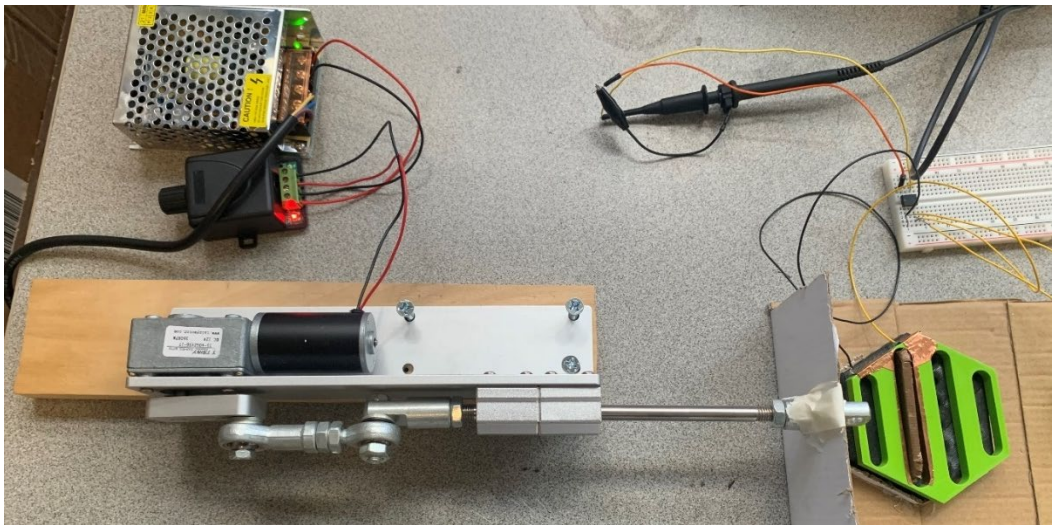

Figure 15. Solid bar design in connection with the linear motion arm.

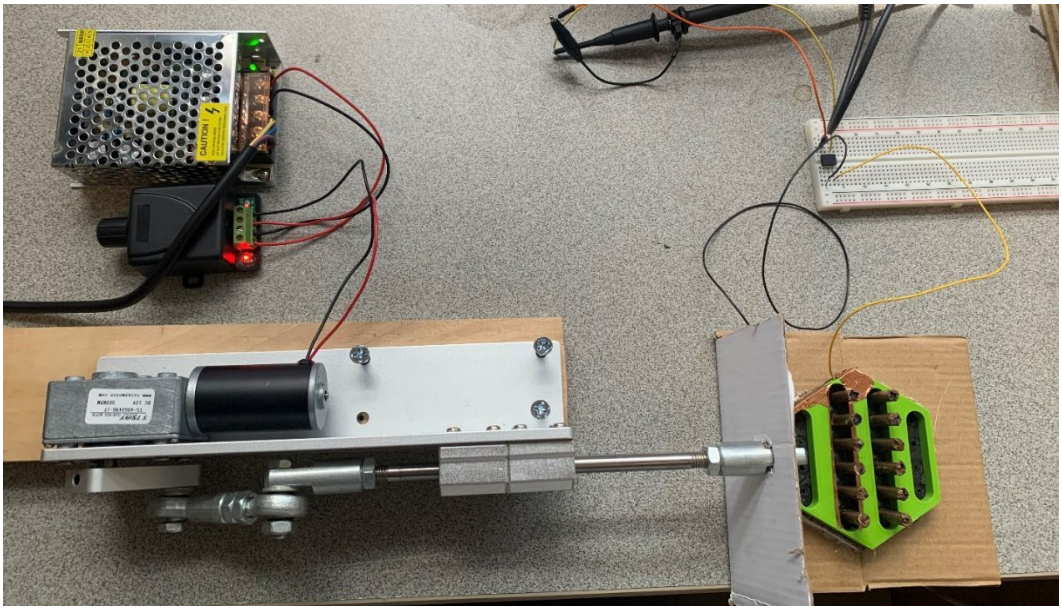

Figure 16. Constant peg design in connection with the linear motion arm.

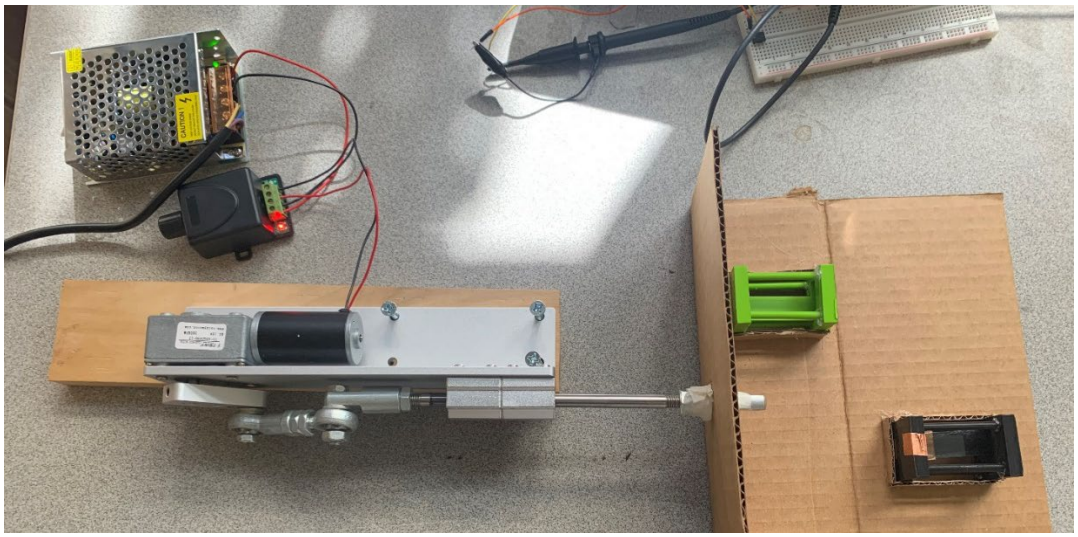

Figure 17. Free bar design connected to the linear motion arm.

Design #4 (Figure 17) was tested with two of the same designs in both series and parallel connection to see which configuration produced the most voltage. Additionally, the designs used both sides, where the PTFE tape was placed on both ends of the free bar and copper tapping was placed on both side of the holder.

V. RESULTS

A. MANUAL EXCITATION RESULTS

The following results are from the manual excitation mode of the hand motion initiating the full contact of the copper tape to the PTFE material that translates mechanical motion to electrical output. Each of the designs described has been tested under similar conditions. Due to the unspecified motion of the manual excitation used, not all devices would undergo the same motion. There is an error associated with this experiment as the motion is generated based on human motion. The constant is the time interval used for each which was a 5s interval.

1. Constant Peg

Design #1, the constant peg device held on a flat surface was manually moved to initiate a voltage output. The device was connected in series to a rectifier on a breadboard with an oscilloscope to record the voltage output. The voltage output is shown in Figure 18. The max voltage produced by the design was 1.5V.

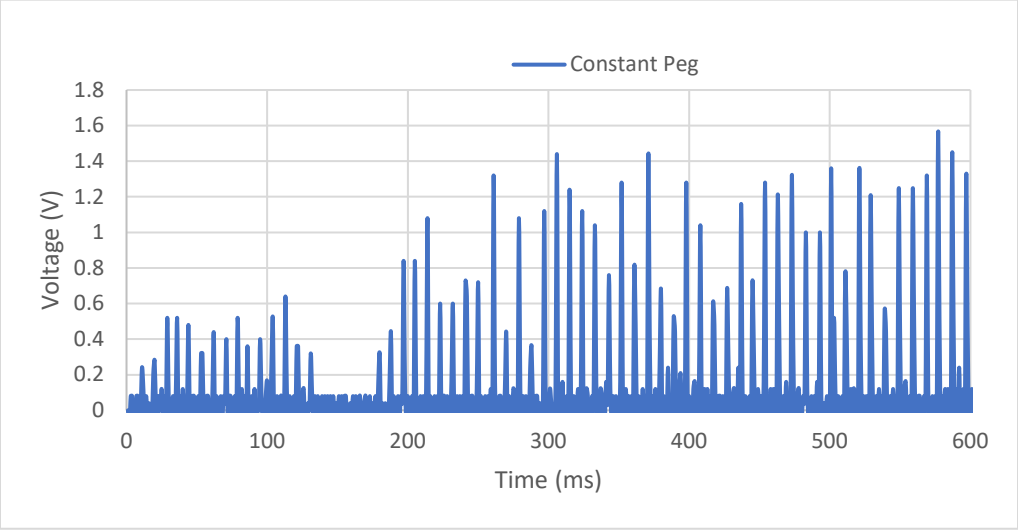

Figure 18. Voltage produced from constant peg design #1 with rectifier in circuit.

2. Solid Bar

Design #3, the solid bar device, was tested on a flat surface where manual motion was applied to the device to produce a voltage output. The device is in series with a rectifier and oscilloscope to record the voltage produced. The max voltage produced by the device was 2.75V, the total test results are shown in Figure 19.

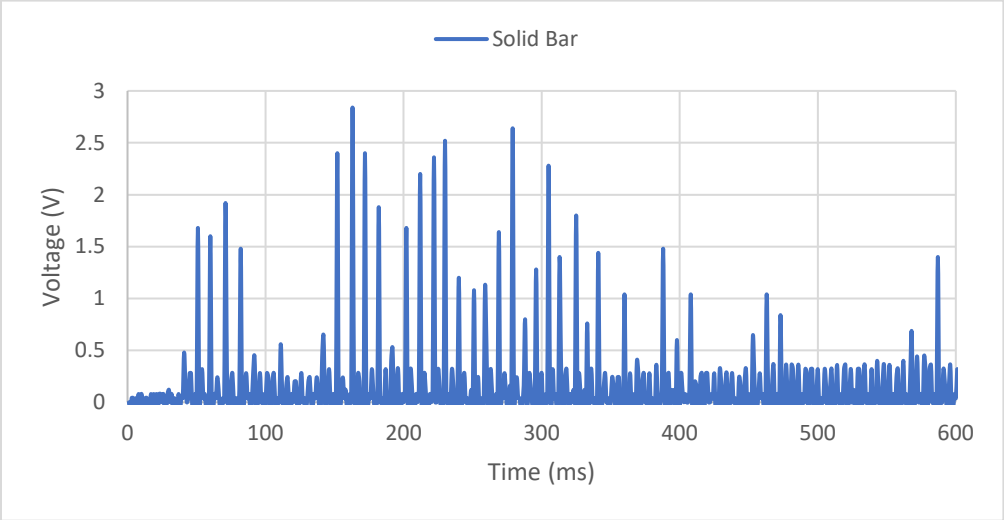

Figure 19. Voltage produced from solid bar design #3 with rectifier in circuit.

3. Free Bar

Design #4, the freely moving rectangular bar device, was tested under manual motion first without a rectifier, then with a rectifier in series. The results without a rectifier are showed in Figure 20. The max voltage produced for this device without a rectifier was 1.00V. A comparison between design #3 and #4 is shown in Figure 20. The comparison between the two designs was done because both use a rectangular bar as an electrode. The difference between the designs is that design #3 the is bar fixed and design #4, the bar is free to move.

Comparing design #3 and design #4, (Figure 20), the two designs showed similar voltage output, but the solid bar design showed higher maximum output of 1.1V while design #4 had a maximum voltage of 0.80V. The comparison test was done separately for

each design after the initial testing runs were completed. The fourth design did not produce the same amount of voltage as previous tests shown but maintained similar results over the five tests conducted under manual excitation. The solid bar design #3 showed a constant voltage with a maximum of 1.1V was produced. The constant voltage produced for the solid bar is seen in the peach color marking and the free bar voltage is seen in the blue where a lower but still constant voltage was produced. Over the same time interval for both designs, the solid bar had more peak voltages on both positive and negative side, when comparing the total surface area between the two designs the solid bar has more contact suggesting that the higher peaks of voltage would be attributed to the higher contact surface area.

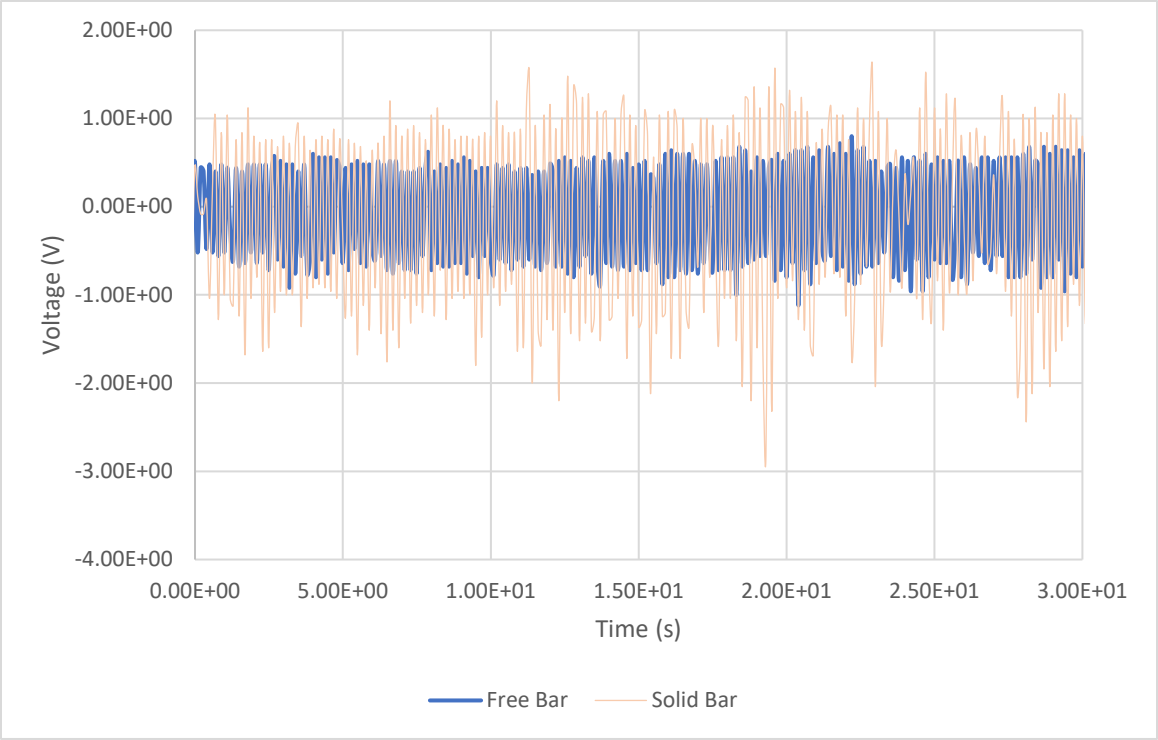

Figure 20. Solid attached bar design #3 versus Free rectangular bar design #4 comparison of voltage production.

4. Manual Excitation with a Rectifier

The use of a rectifier saw an increase in voltage output for the three best performing models, designs #1, #3 and #4. The basic principle of what a rectifier does is that it transitions the input alternating current (AC) into a direct current (DC) output. The rectifier will take the negative voltage produced from an alternating current and convert to a single output in one direction taking those negative voltages adding to the positive voltage. The set up for each design are shown in Figures 21–23 for designs #1, #3 and #4 respectively. The circuit is made up of the TENG wired to the rectifier inputs and the oscilloscope wired to the output of the rectifier to measure the amount of voltage produced.

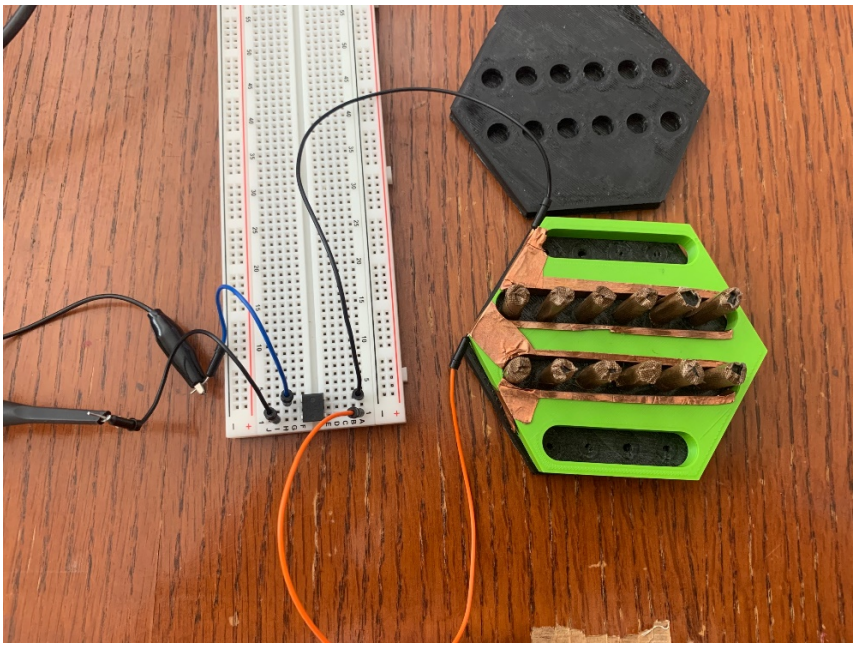

Figure 21. Design #1 in circuit with rectifier and oscilloscope.

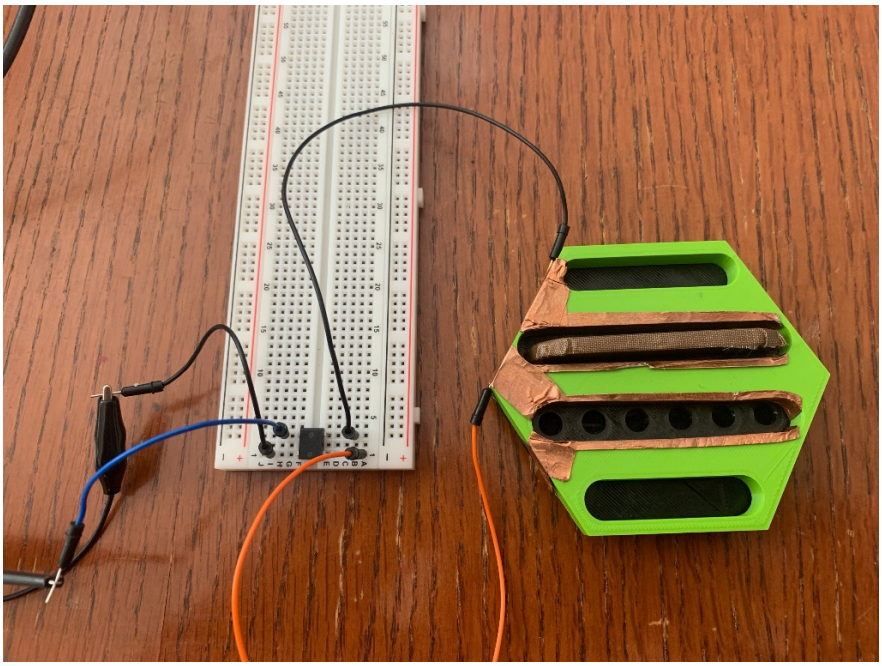

Figure 22. Design #3 in circuit with rectifier and oscilloscope.

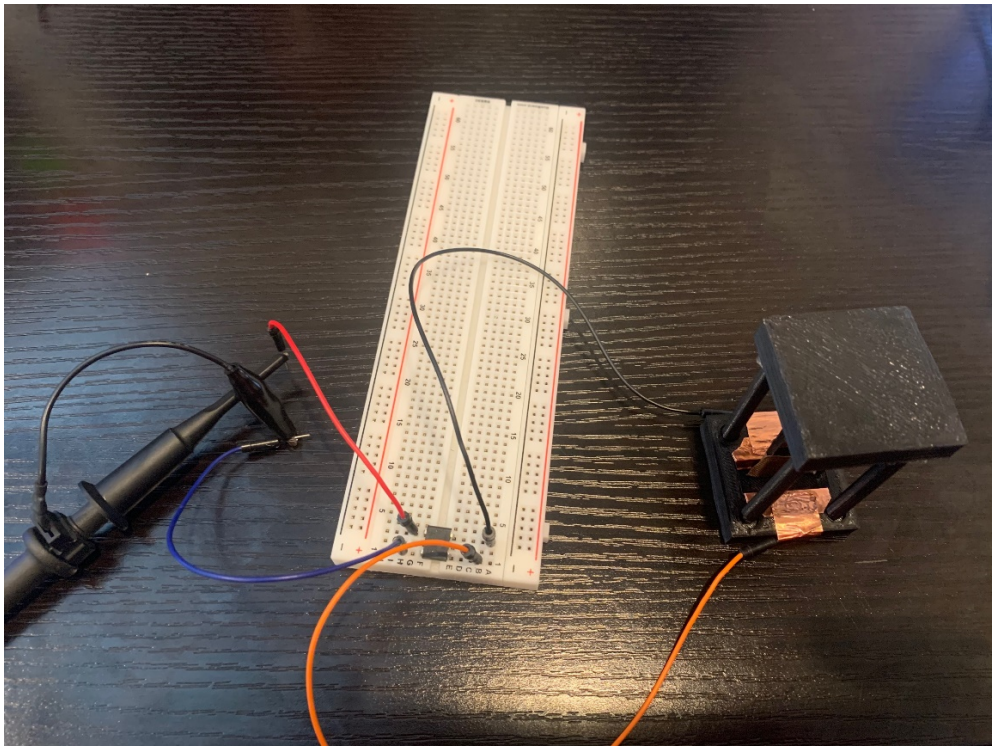

Figure 23. Design #4 in circuit with rectifier and oscilloscope.

Design #1 saw a larger output with a total maximum output of 1.75V but the increase in voltage produced was a small difference to the output without a rectifier. Design #3 saw an increase in voltage output when using a rectifier, with a total maximum voltage output of 2.75V. Design #4 produced a max voltage of 16V when using a rectifier shown graphically in Figure 24. What is also shown in the graph is a constant 5V throughout the testing cycle. The constant 5V was seen in multiple tests while undergoing manual excitation. This was not seen in the other designs when conducting the same tests.

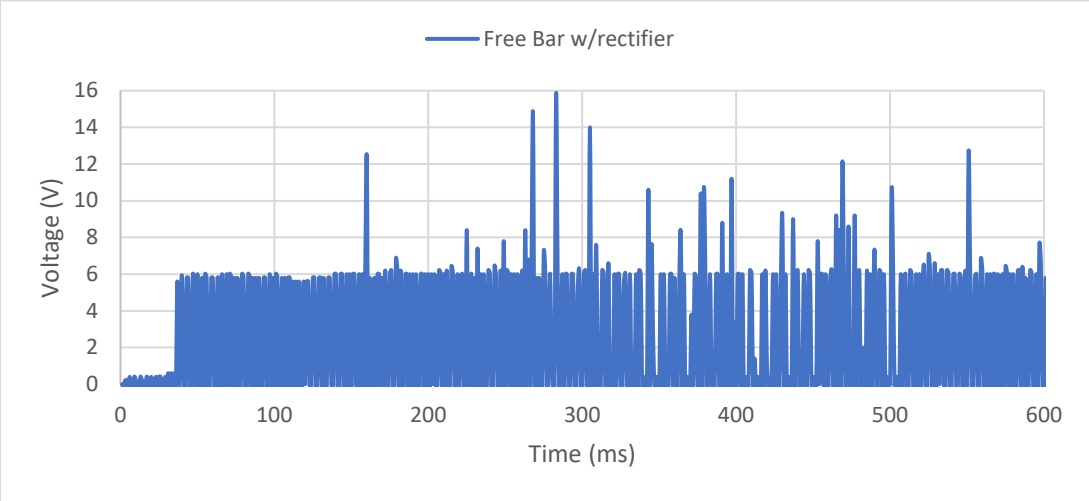

Figure 24. Design #4 voltage output with rectifier in series in circuit, first test run.

B. LINEAR MOTION RESULTS

The second experiment used a linear arm gearbox motor to simulate vibration motion. Each design was connected in series to a rectifier and oscilloscope to measure the voltage produced by the four different speeds of the gearbox.

1. Constant Peg

The constant peg design produced the highest voltage at the full speed of the linear arm motor. The results from each speed are shown in Figures 25–28. The optimum speed for vibration motion is at 1/3 speed. This design had a max voltage of 0.650V at the optimum speed. The highest recorded voltage was produced at full speed with max of

1.34V. The lower voltage at the optimum speed suggests that there may have been not enough contact generated between the two materials. Due to the smaller surface areas of the pegs this could contribute to lower amount of electron transfer leading to a smaller voltage.

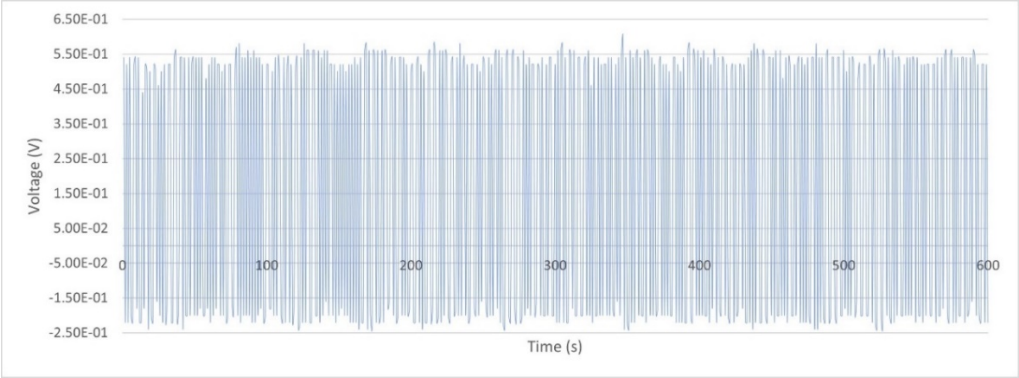

Figure 25. Constant peg design undergoing linear motion at 1/3 speed.

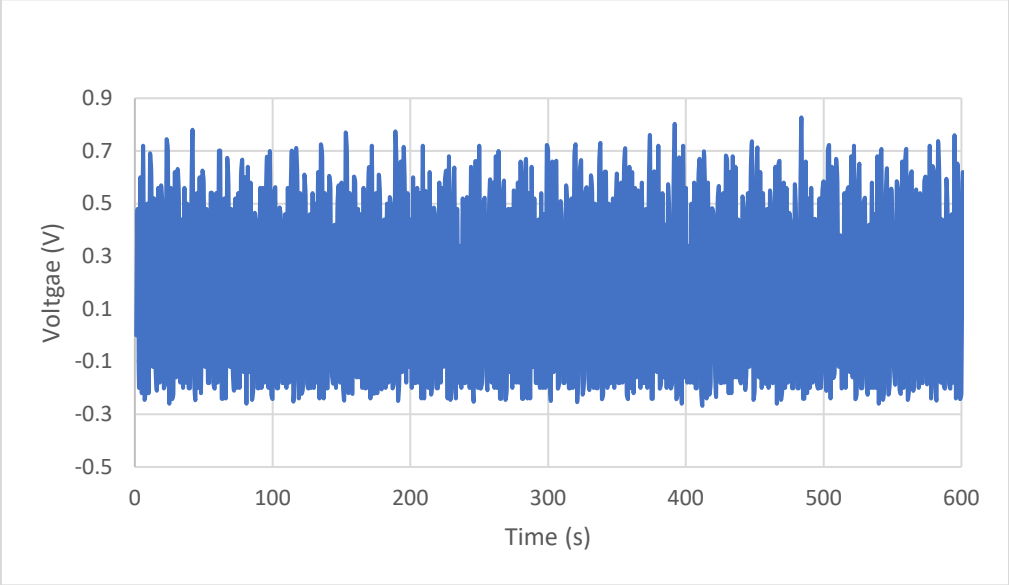

Figure 26. Constant peg design undergoing linear motion at 1/2 speed.

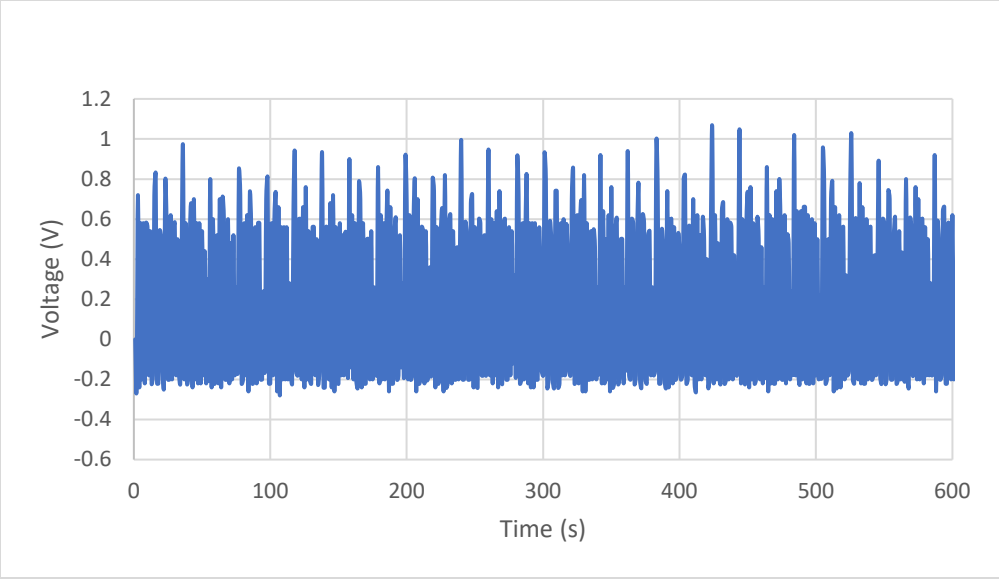

Figure 27. Constant peg design undergoing linear motion at 2/3 speed.

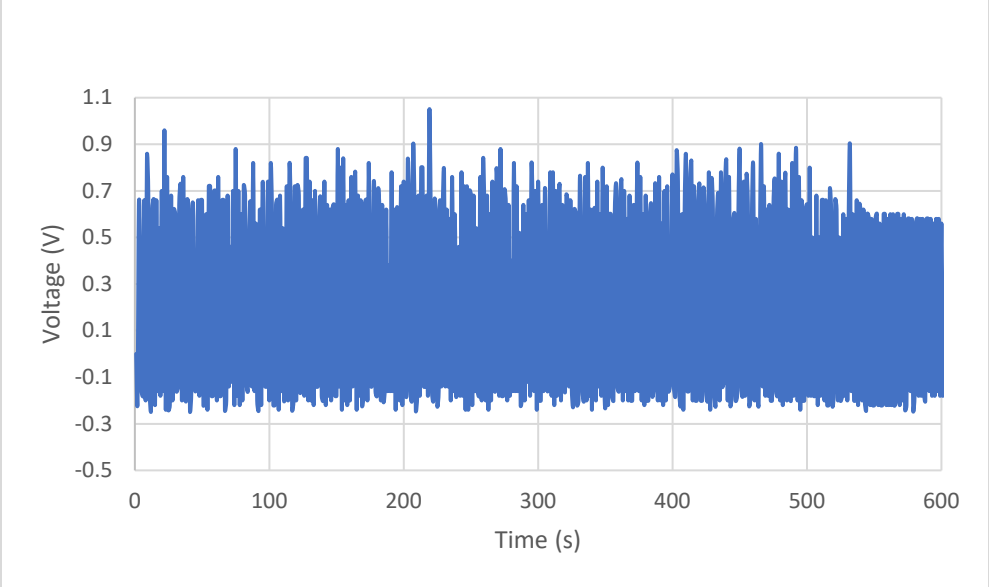

Figure 28. Constant peg design undergoing linear motion at full speed.

2. Solid Bar

The solid bar design was connected to the linear arm gearbox motor as depicted in Figure 15. It was also connected in series to a rectifier and the oscilloscope. The results are shown graphically in Figures 29–32. At the optimum speed of 1/3, the max voltage

produced was 0.650V. The low voltage could be associated with the uneven contact between the bar and slotted middle structure. The small defects and uneven spacing between the two could contribute to lower electron transfer resulting in the lower voltage. Figure 32 shows an uneven voltage produced when operating at full speed. This uneven voltage could be due to the gaps and small defects on the bar preventing even contact.

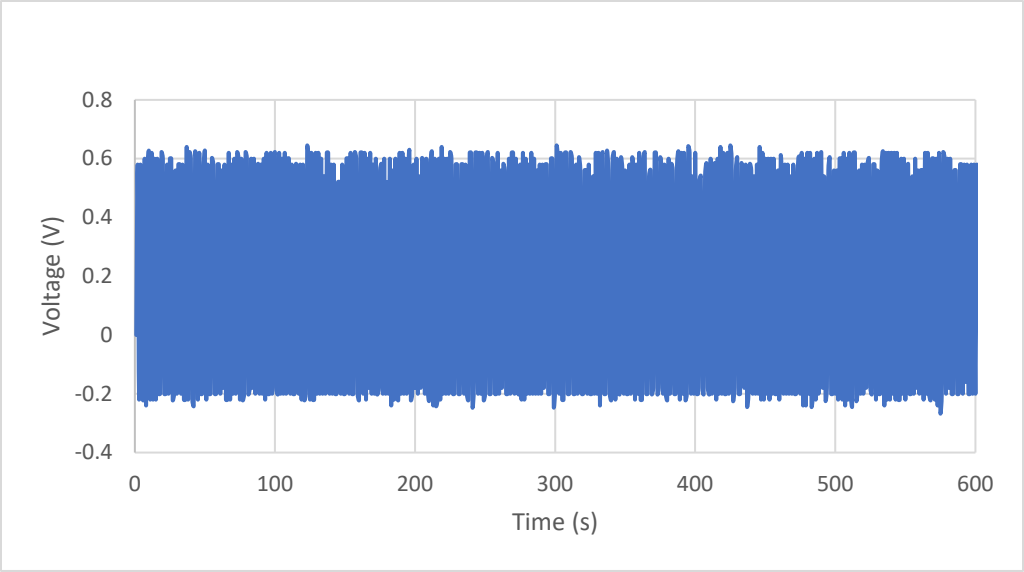

Figure 29. Voltage produced by the solid bar design while undergoing linear motion at 1/3 speed.

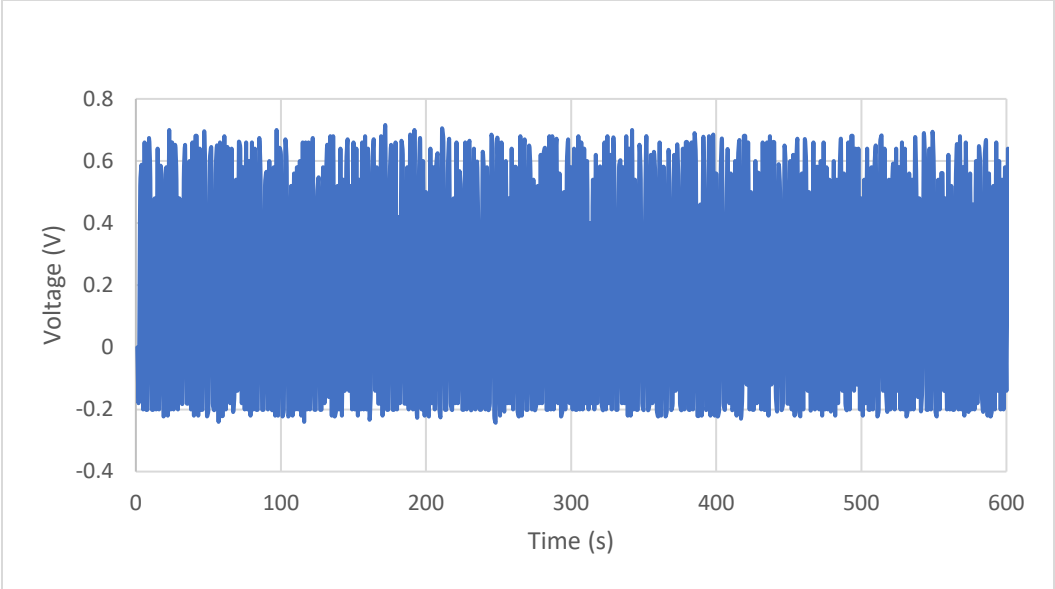

Figure 30. Voltage produced by the solid bar design while undergoing linear motion at 1/2 speed.

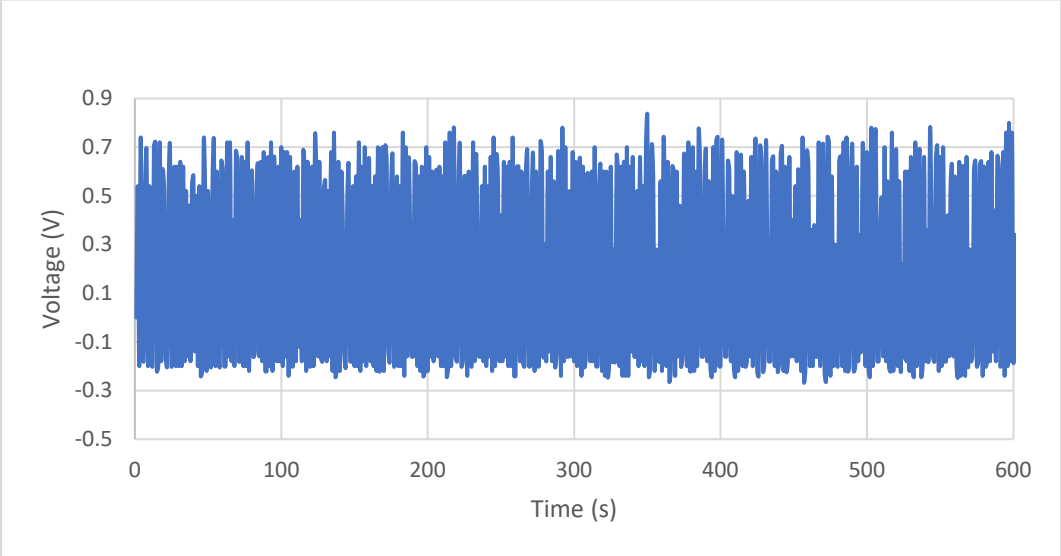

Figure 31. Voltage produced by the solid bar design while undergoing linear motion at 2/3 speed.

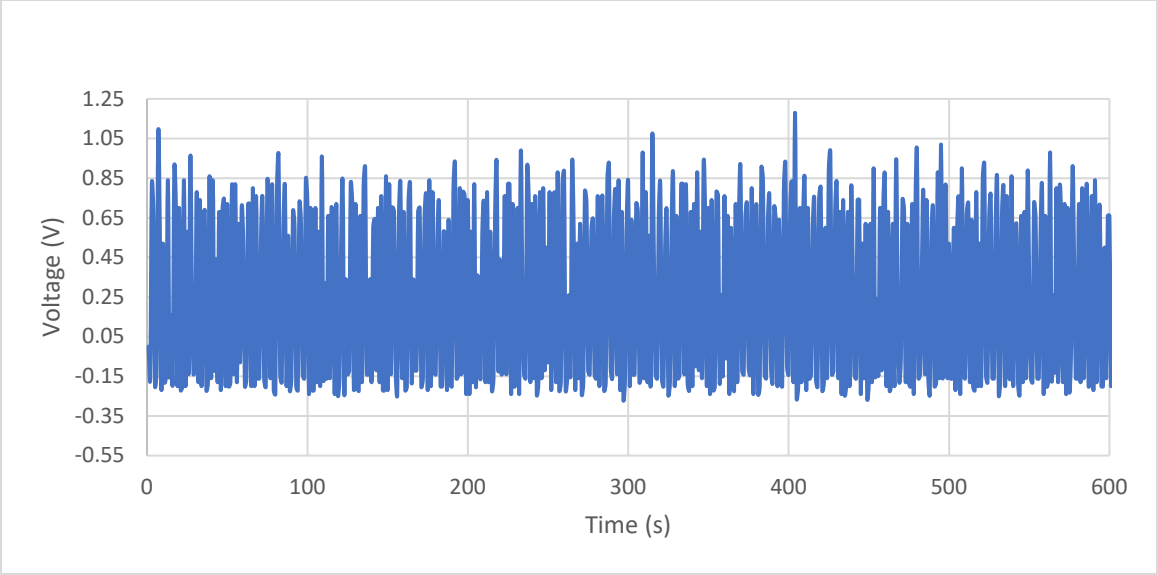

Figure 32. Voltage produced by the solid bar design while undergoing linear motion at full speed.

3. Free Bar

Design #4was connected to the linear arm gearbox motor as depicted in Figure 17. The connection allowed two devices to move together simultaneously. This first testing used one device connected in series with a rectifier. At the optimum speed of 1/3, the max voltage produced was 0.600V. The single unit produced the lowest voltage out of all the designs when using the linear motion device. This design does allow two electrodes to be wired together in series or parallel on one device. When testing this device, the voltage produced increased to a max of 1.23V, as shown in Figure 33. These tests did not show a constant voltage like the manual excitation tests did. Conducting the tests multiple times consistently did not show a constant voltage. The set-up of the copper tape and wires for the design was the same as the manual excitation. The difference was the mode of excitation, but there is not enough evidence to say that this difference is the cause of the constant voltage.

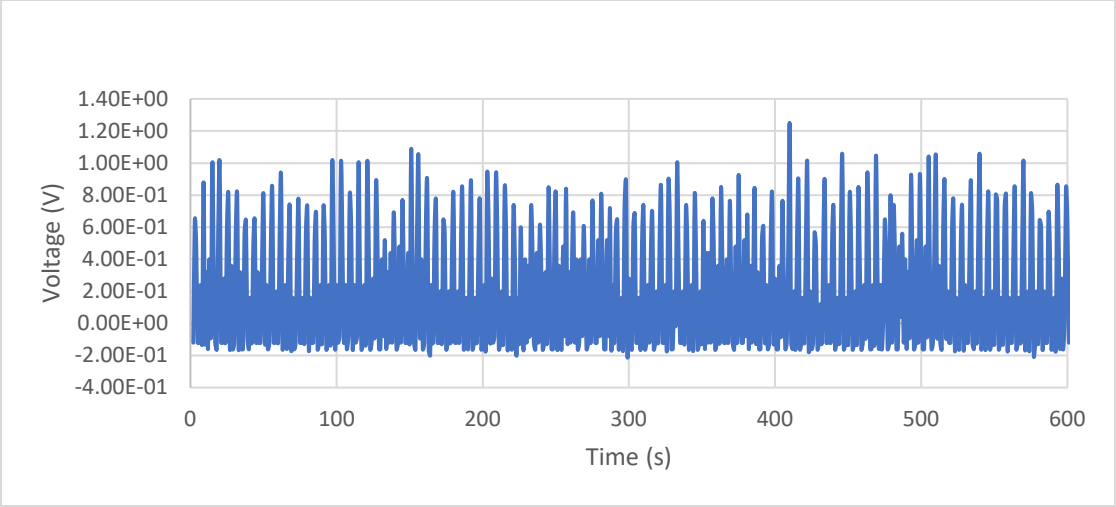

Figure 33. Free bar design with two electrodes connected in series to rectifier at 2/3 speed.

4. Two Free Bar Units in Parallel

The two free bar units in parallel were tested at the optimal speed of 1/3 of the linear motor to show voltage produced for vibration of aircraft wing. The maximum voltage produced was 0.750V. The voltage produced was lower for two units in parallel than one unit using two electrodes connected in series. The lower voltage produced could be due to not enough contact occurring between the bar and block structures indicated by the gaps in the voltage shown in Figure 34.

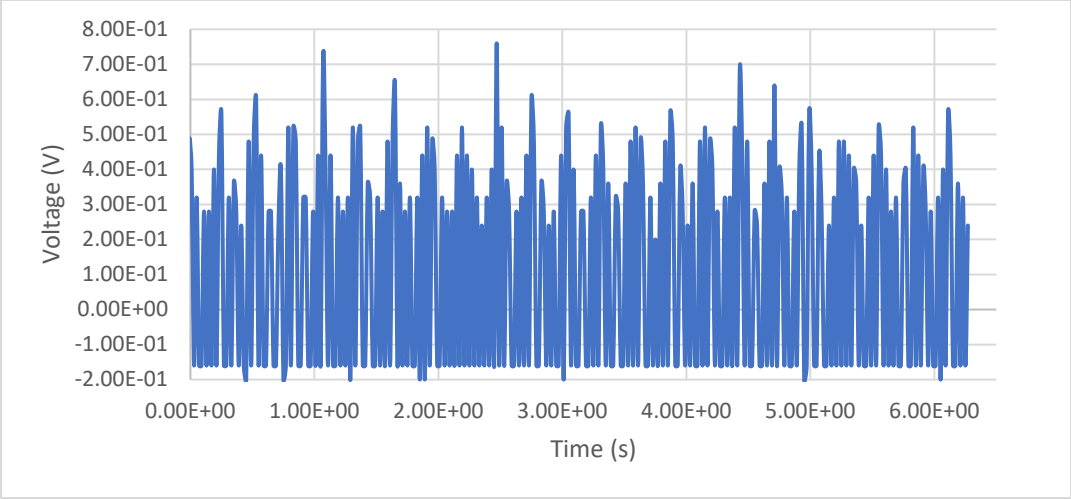

Figure 34. Voltage produced by two free bar designs in parallel connection at 1/3 speed.

5. Two Free Bar Units in Series

The two free bar units were wired in series at 1/3 speed to see the vibration motion of an aircraft wing. The results for two units in series showed a max voltage of 1.40V. The units in series had approx. 0.750V higher than in parallel. Both tests used the two sides of the electrode bar to enhance the contact frequency of the two materials. Figure 35 shows graphically the voltage produced by the two free bar units in series.

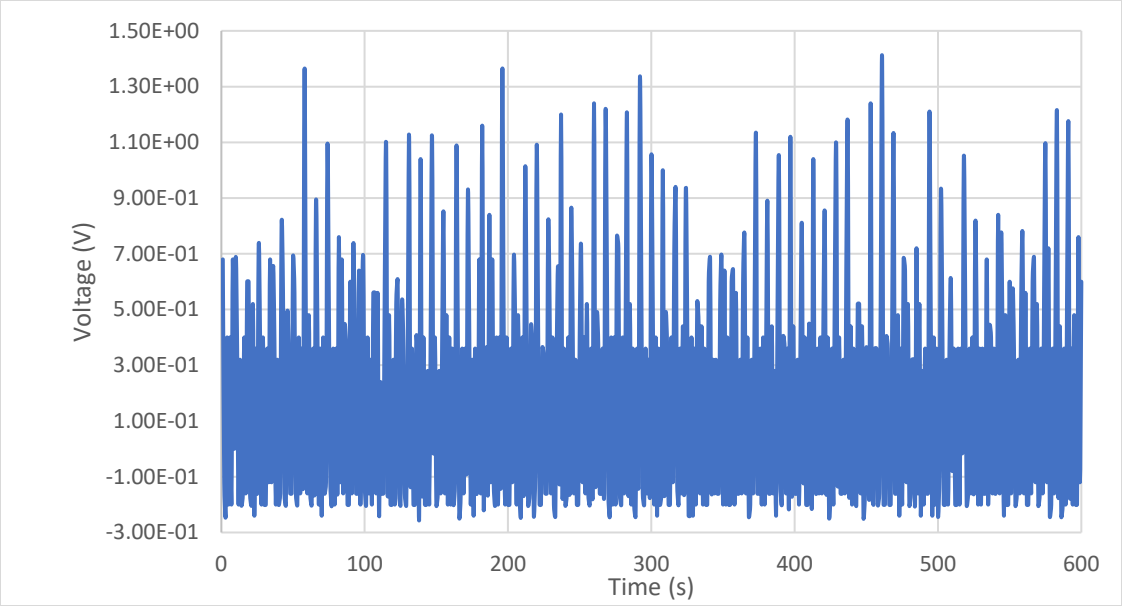

Figure 35. Two free bar units in series at 1/3 speed for the linear arm motion showing graphically the produced voltage.

VI. FEM ANALYSIS OF TENG DESIGN

A. ANSYS MODELLING OF TENG DESIGN

The initial design of the TENG for my thesis used a hexagonal base that had either a fixed rectangular bar or cylindrical pegs and one design that had the cylindrical pegs freely moving on the hexagonal structure. These TENGs produced lower amounts of voltage, ranging from 0.750V to a maximum of 2.10V, where the maximum voltage would not be enough to power a red LED bulb. The highest voltage was seen on the fixed solid bar TENG. To optimize this design, the solid bar was no longer fixed but free to move between two block structures to maximize the contact frequency. The fourth design showed an increase in voltage when undergoing manual excitation, with a max of 16V. To understand how the contact between the free moving bar and block structure occurs, FEM was applied to the structure using ANSYS Transient Structural model analysis.

1. Initial Contact Model Using ANSYS Transient Structural

The analysis setup for the contact modelling for TENG design #4 used the transient structural mode in ANSYS software to show the contact between the block and rectangular bar structures in the design. The initial conditions had zero velocity and no stresses applied to the structure. The ΔT was set to 100ms (0.100s) for 10 steps. The rectangular bar was first set as a free moving structure then set as a fixed end support. An applied velocity in the negative Z-direction was set to the block using the sine frequency function with magnitude of 3mm/s and a frequency of 1.5Hz, calculations are tabulated in Table 2. Figure 36 shows the Full TENG model with the free moving rectangular bar and a velocity applied in the z-direction (labeled as a yellow arrow). Figure 37 shows the rectangular bar with one end fixed (labeled B) and a velocity applied in the z-direction (labeled H).

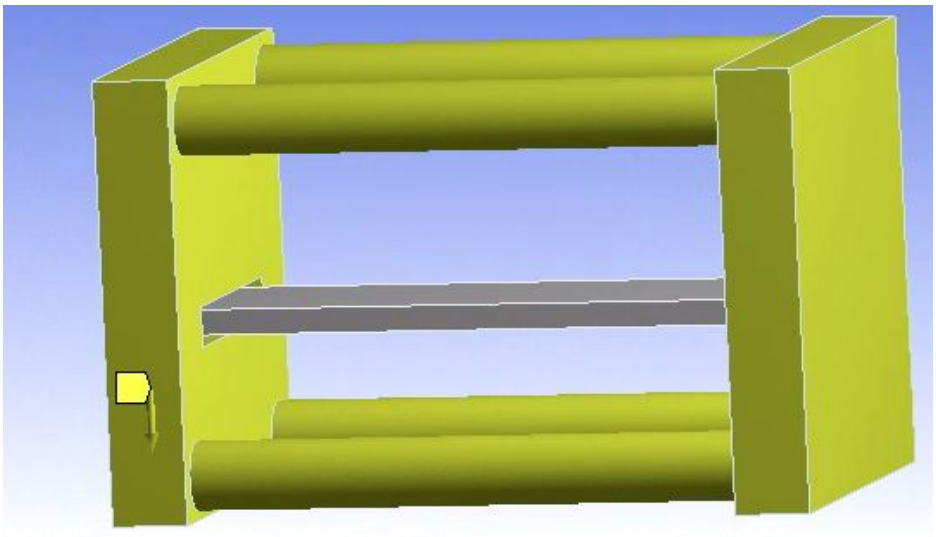

Figure 36. Full TENG model with free moving rectangular bar. The velocity is applied to the outer rectangular block labeled as the yellow arrow in the z-direction.

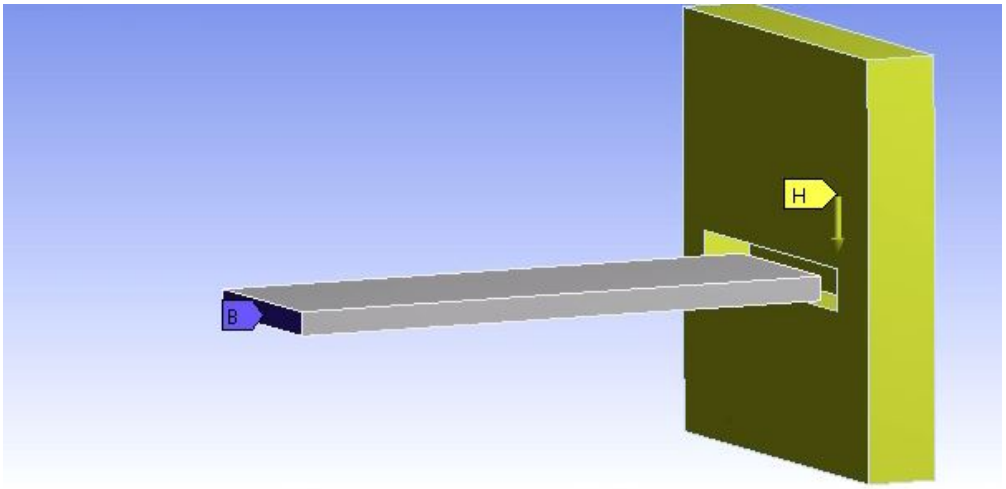

Figure 37. The rectangular bar model with one end fixed labeled B and the rectangular block has a velocity in the z-direction labeled H.

Table 2. Calculated velocity for TENG Design #4 used for contact modelling of the bar and block structures at a frequency of 1.5 Hz.

Time (s)	Velocity=3mm/s omega= 1.5Hz
1.00E-01	2.43E+00
2.00E-01	2.85E+00
3.00E-01	9.31E-01
4.00E-01	-1.76E+00
5.00E-01	-3.00E+00
6.00E-01	-1.77E+00
7.00E-01	9.18E-01
8.00E-01	2.85E+00
9.00E-01	2.43E+00
1.00E+00	1.43E-02

Using a velocity magnitude of 3mm/s and a frequency of 1.5Hz resulted in no contact between the bar and block structures. The maximum displacement of the block was 0.48734mm, shown in Figure 38. The gap between the bar and the block is 1.47mm which is the distance the block must overcome to achieve contact with the bar.

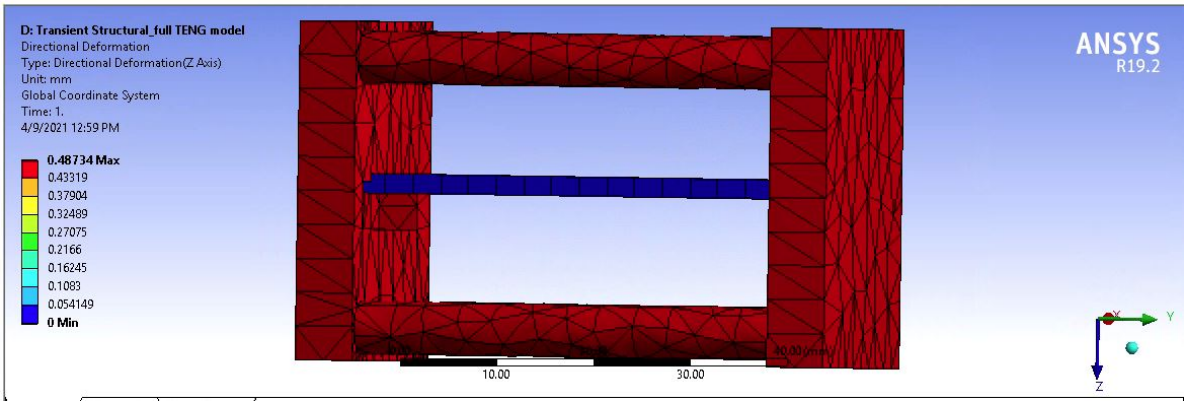

Figure 38. Full TENG design showing contact of the free bar with the block structure done in ANSYS transient structural analysis.

Additionally, the analysis showed a lack of constraints applied to the bar where contact cannot be established between the structures. To compensate for the constraints the bar will be fixed at one end with the other free to move. These constraints will allow the solution to calculate the contact occurring between the tip of the bar and the block structure. Changing the frequency to a slower 0.5Hz should allow contact to occur between the structures. The time interval used was too small to create contact, decreasing the ΔT will increase the number of time steps allowing the block to undergo the velocity longer to initiate contact.

2. Analysis for Fixed Bar and one Block Structure Model

The next analysis configuration had one end of the bar fixed and the other free to move. ΔT was decreased to 50ms (0.05s) which increased the number of time steps to 100 and total time of 5s. The velocity was applied to the block structure under sine frequency function for three different frequencies 0.5, 1.0, and 1.5 Hz all with the same magnitude of 5mm/s.

The first frequency of 0.5Hz resulted in contact between the block and bar with a maximum deformation of 3.2mm in the block. Contact is known to occur because the bar underwent a tip deformation of 1.76mm which exceeds the gap of 1.47mm (Figure 39). The two higher frequencies, 1.0 and 1.5Hz, showed contact was not established because the block was moving at too fast. The maximum deformation gap was 0.0051mm and 1.02mm for 1.0Hz and 1.5Hz frequency, respectively. Since the block did not exceed the gap distance, contact could not be established.

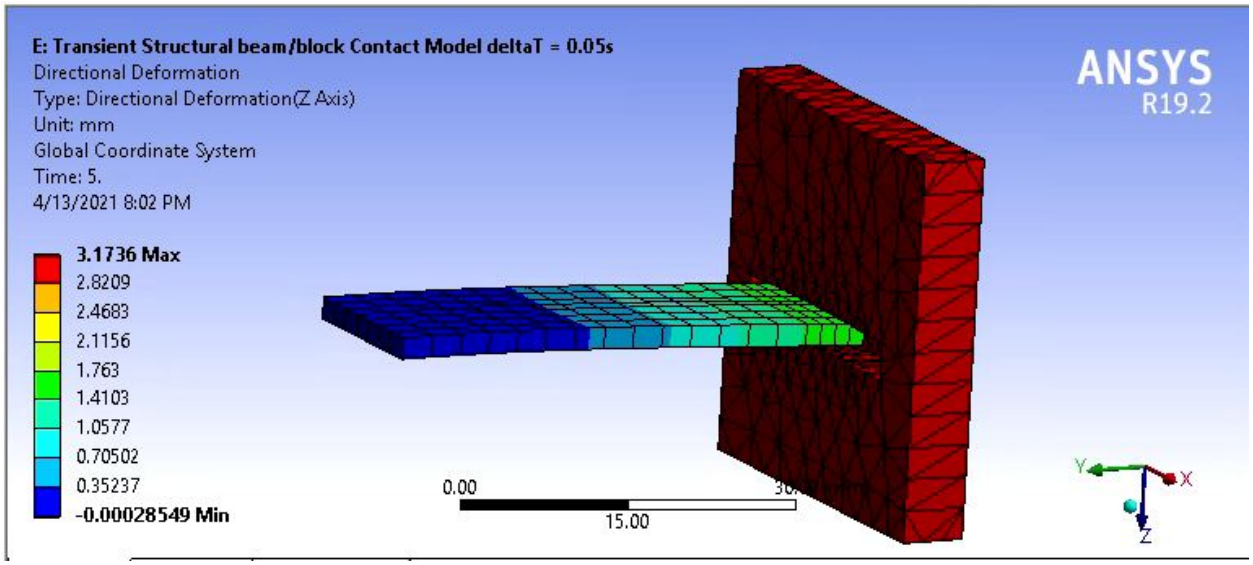

Figure 39. Deformation of the free bar model.

Having shown that the single variable model of the free bar contacts the rectangular slotted holder, the next section shows the contact analysis of the full TENG design.

3. Analysis on Full TENG Model

The analysis for the full TENG design used three different frequency inputs 0.5, 1.0, and 1.5Hz. The rectangular bar was able to freely move as frictionless contact instead of being a fixed support. At a frequency of 0.5Hz and magnitude of 5mm/s, the solution was not able to fully converge (Figure 40). The solution does show a max deformation of the free bar of 0.8664mm, but without the full solution the frequency of the contact is undetermined. Increasing the frequency and the number of time steps would allow more time for the solution to run.

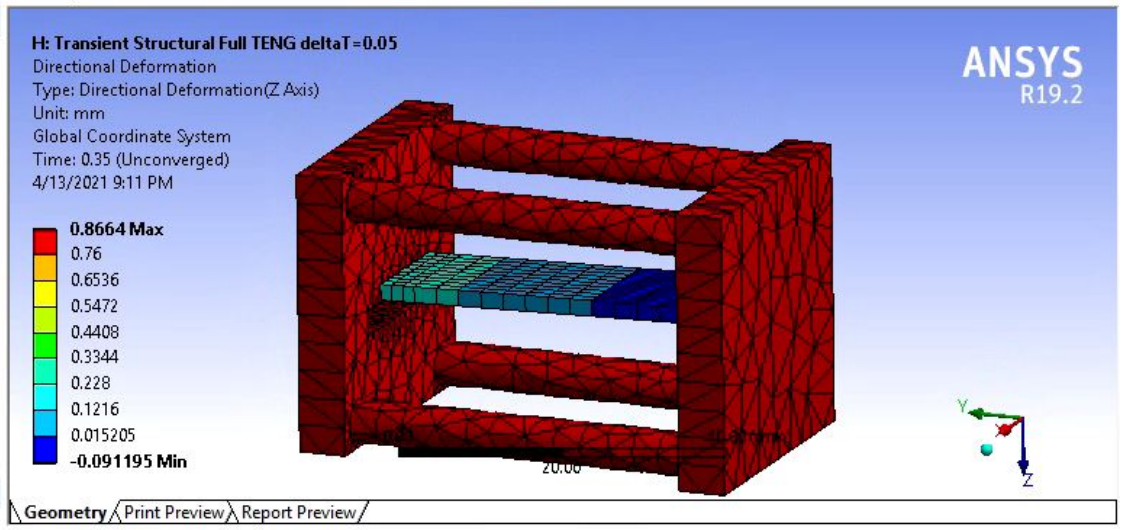

Figure 40. Full TENG contact model deformation of the free bar at 0.5Hz.

The second frequency used was 1.0Hz with a magnitude of 5mm/s. The solution could not converge like the previous results. The un-converged solution suggests that the model does not being have enough constraints given to calculate a solution for the analysis. This means that there is a lack of fixed constraints and there is too much movement of the free bar to model correctly.

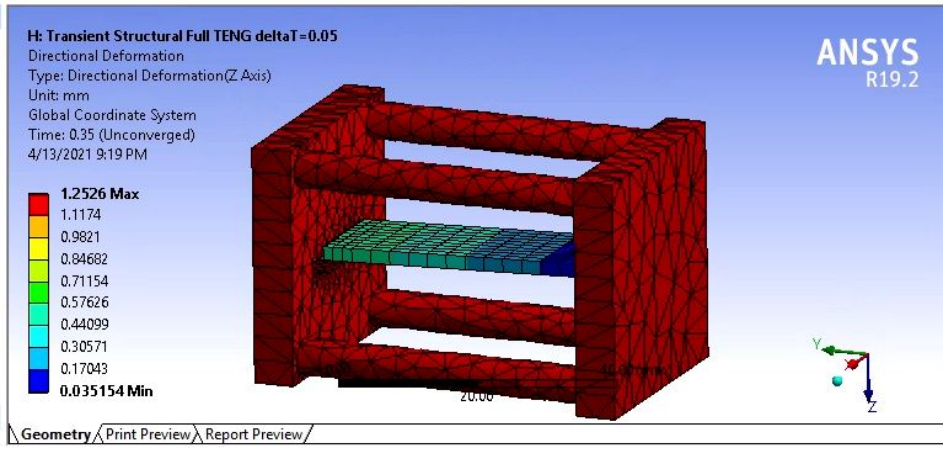

Figure 41. Full TENG contact model for the deformation of the free bar at 1.0Hz.

Since these models did not produce a full solution, the deformation seen is unreliable to determine contact frequency. To get a better solution a smaller ΔT was used at 0.005s (5ms) increasing the number of time steps to 1000 steps. The solution did not converge at 0.5Hz frequency with a max deformation of 1.591mm. To find contact frequency with the full TENG design, nodal deformation analysis will be used.

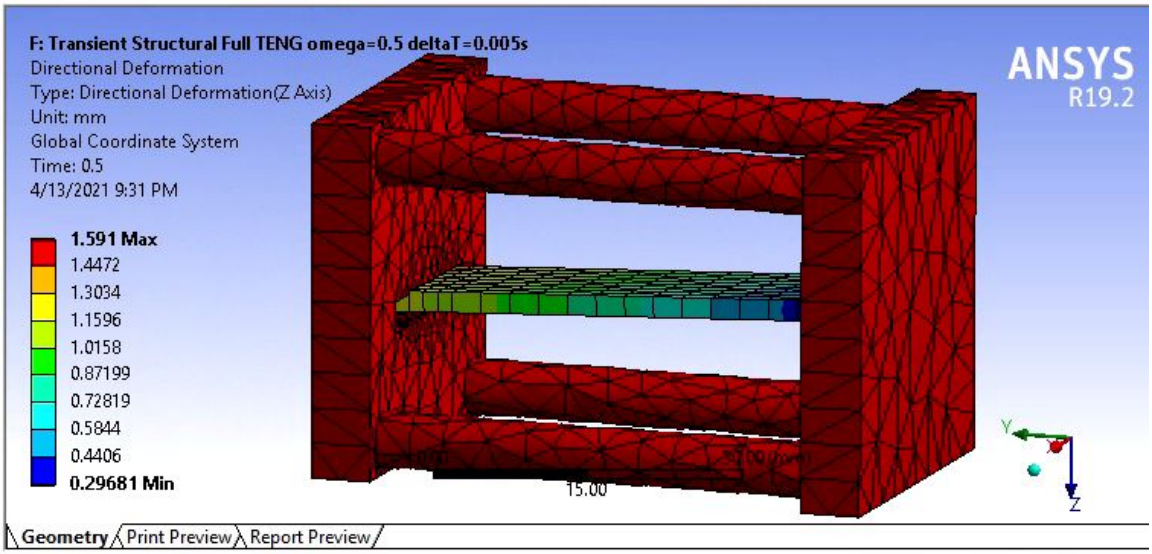

Figure 42. Deformation of the full TENG design with free bar at frequency of 0.5Hz and velocity of 5mm/s.

4. Comparison of FEM to Experimental Results for Fixed Bar and Free Bar Designs

The FEM analysis showed that the fixed bar model contacted the block structure because the deformation exceeded the gap distance between the two. The structure underwent a maximum deformation of 2.5mm at the tip, which exceeds the gap distance of 1.47mm. Using a frequency of 0.5Hz at a low velocity of 5mm/s showed a contact frequency of 1 contact per second. The contact occurred at the tip of the bar and the top and bottom of the slotted area in the block structure. The time interval was set to a length of 5s, doubling the length would increase the contact per second which suggests an increase in voltage produced for the design.

The free moving bar design had smaller contact frequency occurrence, about less than 1 contact per second. The free moving bar had no constraints, so the bar was able to move on both sides. This allows for two electrodes to be used with the design unlike the free bar design that has only one electrode source. The FEM analysis showed that for either side of the bar there was lower number of contacts per second. The maximum deformation seen on the bar was at the left end at 1.304mm. The deformation does not exceed the gap between the bar and block structure. The small deformation means little to no contact occurring which suggests low voltage production. At the same frequency and velocity, the free bar has lower number of contacts than the solid bar design.

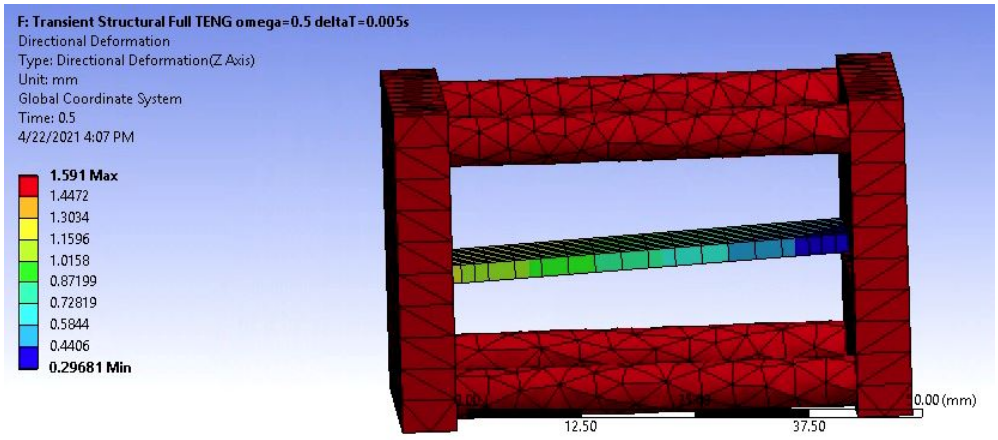

Figure 43. Contact model analysis for Free Bar TENG design at 0.5Hz and velocity 5mm/s.

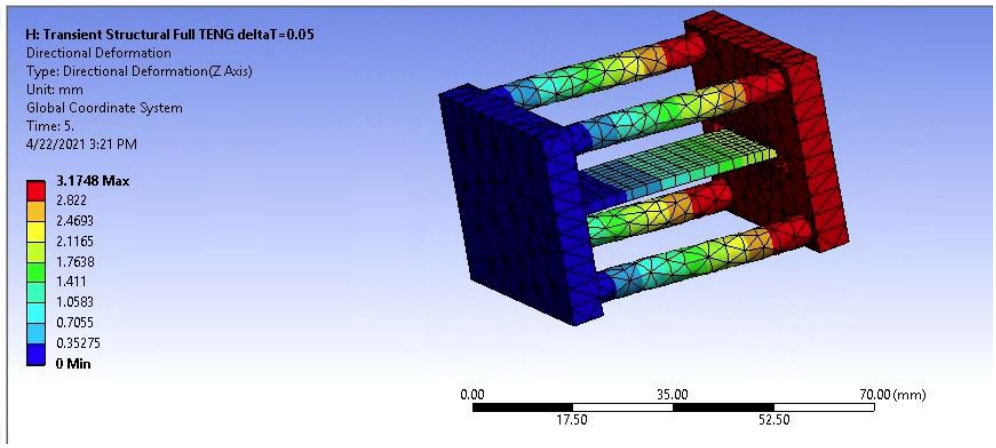

Figure 44. Contact model analysis for Fixed Bar TENG design at 0.5Hz and a velocity of 5mm/s.

The experimental results for the two designs, fixed and free bar, showed similar contact results with the fixed bar producing a higher voltage than the free bar. The maximum voltage produced was 1.18V using linear motion excitation at full speed with a rectifier connected in series. The free bar saw a slightly lower voltage of 1.05V produced under the same conditions. The difference in the voltage could be associated with the lack of contact frequency occurring in the free bar as shown in the FEM analysis. The FEM analysis showed that the fixed bar had higher contact frequency. When comparing to the experimental results the higher voltage produced was the solid bar design coinciding with the FEM analysis.

5. Nodal Deformation Analysis

The natural frequency of the bar structure influences the contact with the block structure. Adjusting two specific factors in the natural frequency equation can either increase or decrease the frequency. These two factors are the stiffness and mass. In ANSYS, the factors equate to the elastic modulus and mass density for the material chosen. Two model set ups will be analyzed to understand the contact behavior between the two structures which gives an indication on how effective the design is at producing electricity. The first model will be setting the stiffness to $1.5x10^{11}$ Pa as the high value and $4x10^{8}$ as the low value while holding the mass constant. The second model will hold stiffness

constant and change the mass to 5 kg/mm^3 as a high value and 5x10^{-5} kg/mm^3 as a low value. The same initial conditions will be applied to the four models with a velocity of 5mm/s at a frequency of 0.5Hz for a time of 5s at a ΔT of 50ms (0.05s).

To understand the contact frequency of the device under these conditions, nodal points on the tip of the bar and top and bottom of the slotted block structure will be analyzed looking at their deformation to show contact between the two structures. The nodes chosen were parallel to each other with respect to their position on the bar and slot of the block.

When changing the stiffness of the bar to a higher value of 1.5x10^{11} Pa and holding the mass constant the natural frequency of the bar increased based on the equation for natural frequency given below:

$$\omega_n = \sqrt{\frac{3EI}{\frac{L^3}{m}}} \tag{2}$$

where E is the material stiffness, I being the moment of inertia, L is the material length, and m is the mass. When increasing the stiffness, the overall frequency increases. When increasing the density, the overall frequency then decreases. The contact generated for this model resulted in top contact period of 0.65s duration for a frequency of 3 cycles and a bottom contact period of 0.9s for a frequency of 2 cycles over the 5s time interval. Figure 45 shows the contact start and stop for the top node of the bar and top node of the slotted block structure. The higher the stiffness value showed a contact frequency like what was seen in the experiment where the number of contacts made was higher producing voltage. The bottom of the structure for contact frequency is shown graphically in Figure 46.

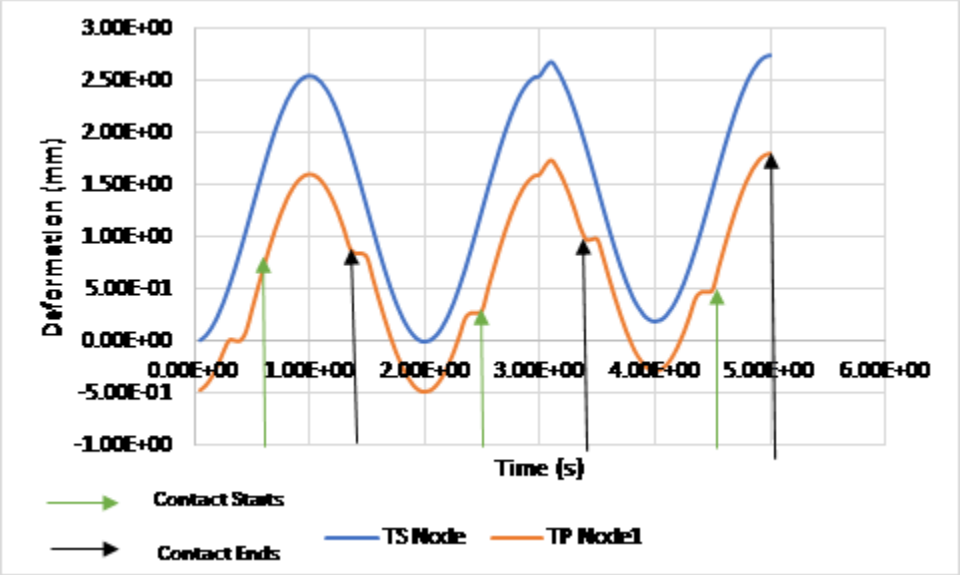

Figure 45. Contact model analysis for bar stiffness of $1.5x10^{11}$ Pa showing contact start (green arrow) and contact end point (black arrow) for the top bar node (TP Node1) and top slot of the block node (TS Node).

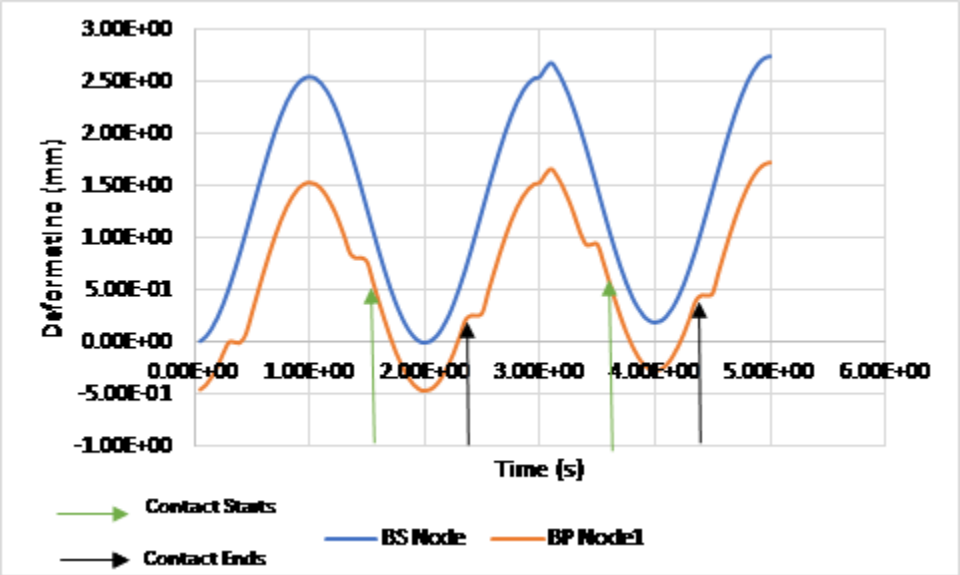

Figure 46. Contact model analysis for bar stiffness of $1.5x10^{11}$ Pa showing contact start (green arrow) and contact end point (black arrow) for the bottom bar node (BP Node1) and bottom slot of the block node (BS Node).

When changing the bar stiffness to a low value of $4x10^7$ Pa, the contact varied such that the period of contact for the top of the bar to slotted block structure was 0.15s for a frequency of 6 cycles. The bottom contact period was 0.25s with a frequency of 3 cycles. The shorter contact time with an increase in frequency shows that at a lower stiffness the higher contact occurs with more contact on the top of the bar than the bottom. Figure 47 shows the contact start and end frequencies for the top of the bar and slotted block structure.

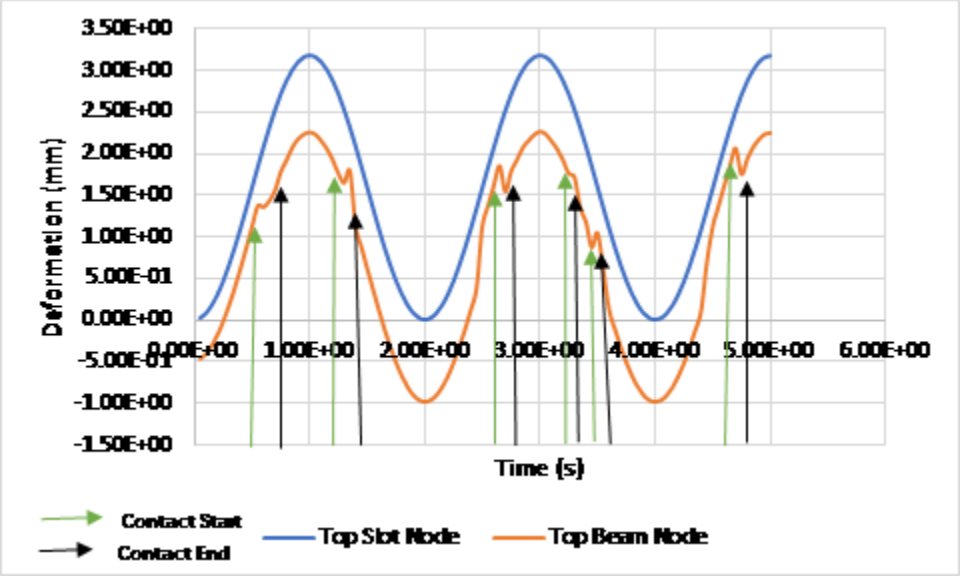

Figure 47. Contact model analysis for bar stiffness of 4 x 10^7 Pa showing contact start (green arrow) and contact ends (black arrow) for the top bar node and top slot node of the block structure.

Changing the density of the bar vice the stiffness showed different results. First when changing the density to a smaller value of $5x10^{-5}$ kg/mm^3, the contact time was approximately 0.15s with a frequency of 5 cycles for the top of the bar. Figure 48 shows the contact start and end time graphically. The bottom of the bar had a smaller frequency of 2 cycles with slightly larger contact time of 0.25s. The total contact time for both the top and bottom of the bar was 0.75s out of the 5s interval, and there was a larger amount of time where no contact occurred. The lower contact time could be due to the larger ΔT of 50ms where contact occurring at shorter time intervals were not modelled and lost in the calculations.

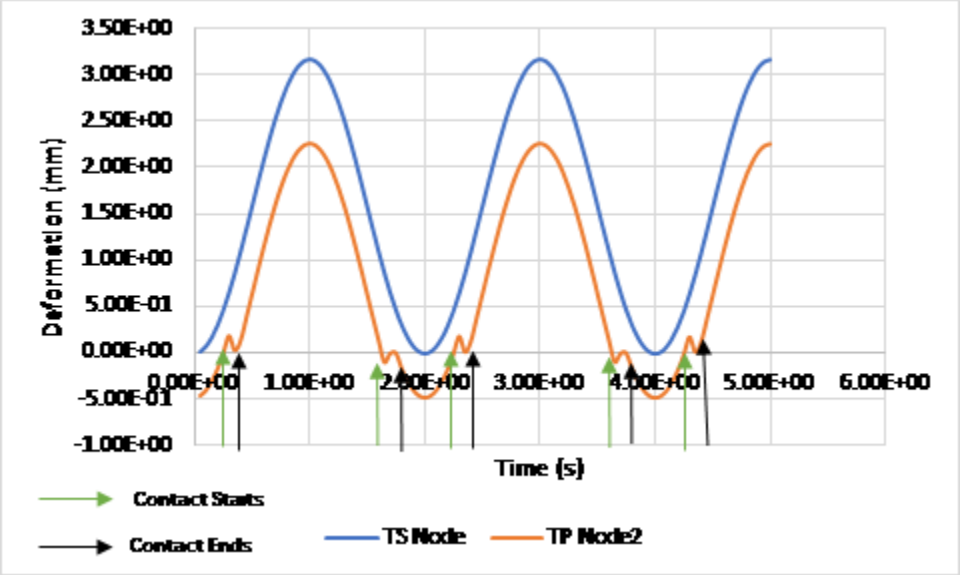

Figure 48. Contact model analysis for bar density of $5x10^{-5}$ kg/mm^3 showing contact of the top bar to the slotted block structure.

At a higher density of 5 kg/mm^3 the bar reacted in a different mode than the previous model. The bar shifted mode frequencies as the block contacted the bar. The contact time was smaller, approx. 0.10s per contact, but a higher frequency of 7 cycles. Figure 49 shows the contact start and end time for the top of the bar and slotted block structure. The contact time for the bottom of the bar to hit the bottom slotted block was approx. 0.08s per contact and occurred 6 times. The lower contact time of the bottom structures could be due to the different mode frequencies occurring in the bar as contact was made on the top then translating throughout the time interval.

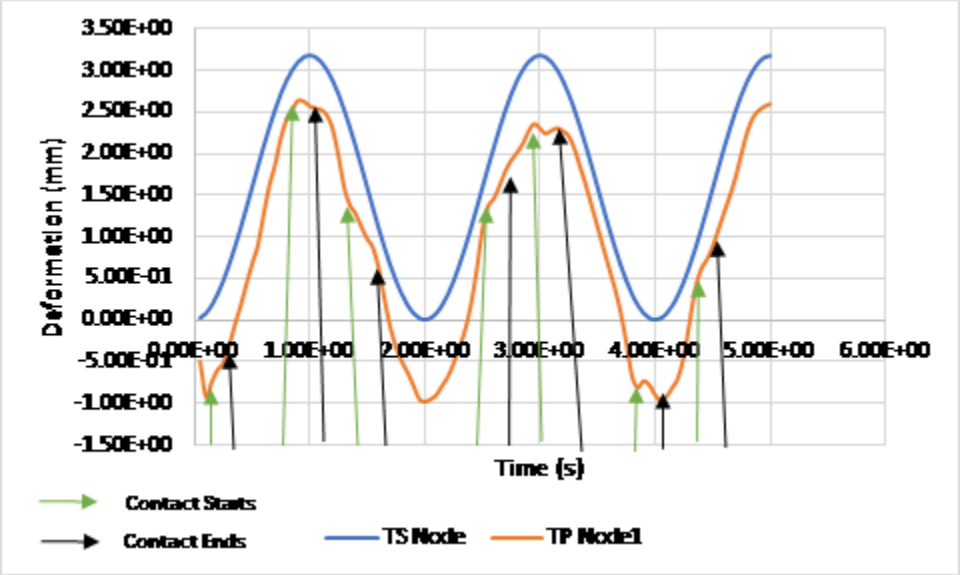

Figure 49. Contact model analysis for bar density of 5 kg/mm^3 showing contact start and end time of the top bar with the top of the slotted block structure.

Overall, the contact time between the bar and slotted block structure was longer when changing the stiffness to a smaller value while holding the mass constant and setting the density to a larger value while holding stiffness constant. When the bar has a smaller stiffness, there is less resistance to bending deformation. This increases the contact separation between the two structures because the bar is less rigid allowing for more separation to occur. When having the stiffness set to a larger value, the contact time increased but frequency of contact decreased. This makes sense in that with a higher stiffness value there is less flexibility in the bar with more rigidity preventing separation to occur when contact is initiated.

Changing the density to a higher value resulted in an unexpected mode change in the bar. As contact was made on the top of the bar, the mode changed throughout the bar, this change decreased the contact time but increased its occurrence. The smaller density saw similar results to a higher stiffness with longer contact time but shorter frequency of occurrence suggesting that having a denser material with small stiffness would induce a higher number of contacts/second and contact duration. The contact duration is how long

the contact occurs. With a higher duration there is more contact meaning more voltage produced. A smaller duration then a lower voltage is produced.

The smaller density value for the top of the bar had a contact duration of 1 second and the bottom contact duration was 0.40 seconds. At a higher density value, the contact duration for the top of the bar was 1.4 seconds and the bottom of the bar had a contact duration of 1.2 second.

This parametric study shows the validity to having design #4 produce voltage through contact separation and functions as a working TENG. For the TENG to operate efficiently, a high number of contacts along with high contact duration needs to occur. According to the analysis, having a denser material will have higher contact duration above 1.5 seconds. To optimize this design, changing key material properties can increase and decreases the contact duration. The performance of the fixed bar in this study showed a more even distribution of contact between the two structures and when changing either the stiffness or density there was a change in contact frequency. A smaller stiffness increased the contact frequency showing that the material reacted more to the velocity and created more contact between the two structures. When changing the density to a higher value, higher contact frequency occurred like having a small stiffness value. To optimize the performance of design #4, this analysis showed that the material properties dictate contact frequency.

THIS PAGE INTENTIONALLY LEFT BLANK

VII. SUMMARY

A. CONCLUSIONS

The experiments done to the four TENG designs showed that two of the designs were viable options in harnessing the vibrational motion, design #3 and #4. Both designs used a rectangular bar with an outer structure initiating contact to the bar to generate a transfer of electrons between the PTFE and copper tape. Design #3 had the rectangular bar fixed to a hexagonal plate and design #4 had the bar freely moved. The fixed bar produced a higher overall max voltage than the freely moving bar. The design however failed to produce a consistent voltage to power a red LED bulb, this shows that there are flaws within the design as the red LED requires the smallest amount of voltage, 2.4V. For these two designs the concept for producing voltage is to have the copper tape on the block structure contact the PTFE of the bar structure multiple times at higher frequencies to induce large electron transfer. To find how contact occurs in the design, a parametric study was done using implicit software modelling. The parametric study found that the contact frequency of the free bar was difficult to model for the varied contact of the free bar when contact was initiated. This was shown in the experimental results that showed a lower voltage output than the fixed bar suggesting that the frequency of contact of the free bar was lower at the steady velocity output roughly 60RPM. What was seen for the fixed bar model was the contact was higher than the free bar design. The fixed bar was able to model correctly at different velocities showing that this design was able to contact the block structure multiple times over the time interval indicating the higher voltage output would be produced. This is concurrent with the experimental data where the fixed bar resulted in a higher voltage output approx. 3V was a max voltage produced. The contact initiated by the block structure moves at a more consistent velocity which allows for further electron transfer to occur producing higher voltage output.

Overall, the designs developed in this thesis to harness vibrational energy from an aircraft wing were able to produce voltage but at a low output than what would be required to produce sufficient electricity. The design that saw the lowest output was the free moving peg, design #1, where the pegs were not able to freely move at a high rate to create enough

electron transfer between the PTFE and copper tapes. The strength of the design also failed when tested at higher velocities where the pegs would separate from the design. When having the pegs fixed to the bottom structure the design was able to produce more voltage because the PTFE on the pegs was making enough contact to the copper tape of the block structure producing enough electron transfer. However, this design saw low voltage produced, one reason for the low voltage is the amount of surface area available for contact between the PTFE and copper tapes.

To achieve a higher voltage production changing the design by increasing the surface area of the PTFE tape would then enhance the electron transfer between the two materials. Design #3 increased the surface area of the PTFE tape by using a rectangular bar fixed to the bottom structure. The voltage produced with the fixed bar design increased by 2V from the previous two designs. This shows that increasing the contact surface area of the PTFE tape allowed for more electron transfer between the materials leading to a higher voltage produced. A design flaw in this was the ability for the copper tapes, structure to fully contact the PTFE evenly at one time, because of 3-D printed defects in the bottom structure contact would not be even at any one time reducing the amount of voltage produced. Taking design concepts from design #1 with free pegs, the fourth optimized design used free bar moving in a block structure to enhance the contact frequency between the two materials. The free bar design would allow for a more even contact to occur between the materials and add another side of the materials where each side of the bar and block structure had PTFE tape and copper tape, respectively. Experimentally what was seen was a lower voltage than the fixed bar, approx. 1V lower output was seen. Even when putting both sides of the structure in series the voltage produced was approx. 0.450V higher than only one side connected. When using multiple units of the free bar in series there was a higher voltage produced approx. 1.40V. Two units in parallel saw a lower voltage of 0.750V for a max showing that when in series there is a higher voltage produced for the free bar design. This optimized design did not produce as high a voltage as the fixed bar design which was unexpected due to the contact ability for two sides of the free bar to create contact of the materials. When testing the two designs for electrical output with an LED bulb neither design would produce enough consistent voltage to light the bulb

showing that these designs even though produced voltage did not have a consistent high voltage that allowed for electricity to flow properly.

In conclusion, the developed TENG designs can be optimized to increase their contact ratio by changing the mechanical properties such as density and stiffness. When changing the density to a higher value the contact time ratio increased to 1.4 contacts/second. The increase in contact time will have a direct impact on the voltage production because it increases the electron transfer for the triboelectric effect.

This study only used one or two designs for testing. The testing results showed one design produced a small amount of voltage, but with multiple units wired in series the voltage production will be higher. This was seen when two design #4 units were wired in series and the voltage difference from one unit to two was 1V higher. Increasing the number of units to just 4 units would add an additional 2V. Additionally, the available surface area for the design did not allow for high electron transfer and contributed to low voltage outputs for design #3. When changing the design to have higher surface area, 3-D printed defects were found where the lack of full contact between the material prevented proper transferring of electrons reducing the voltage. Finally, the material chosen for the free bar did not allow the vibration velocity to create enough separation for contact to occur more frequently for high voltage to be produced. Overall, these designs proved their use in harvesting vibrational energy with design #4 having the most validity. Design #4 can use two electrodes on either end which increases the voltage produced. Additionally, the design itself can use two or more units. Further research into how multiple units wired in series and used as the base structure is need.

B. FUTURE RESEARCH

The research conducted for this thesis showed that to harness vibrational energy using a sandwich structure TENG with contact separation mode there needs to have flexibility for the chosen material to allow contact between the two structure to occur. Additional research for the free and fixed bar designs can be done using ANSYS with a UAV wing frame structure with multiple designs imbedded within the frame. The frame can then undergo a sine function velocity to observe how multiple designs interact as a

solid frame structure. Also, a redesign of the free peg TENG can be done like the free bar design to see if just one peg will produce a more even voltage distribution. This will show that there is a difference in contact frequency between a cylinder peg and a rectangular bar.

LIST OF REFERENCES

[1] Wang L. Z., "Triboelectric Nanogenerators as New Energy Technology and Self-Powered Sensors—Principles, Problems and Perspectives," 2014, Faraday Discussions, 176, pp. 447–458, DOI 101039/c4d00159a.

[2] Wu C., Wang A. C., Ding W., Guo H., Wang Z. L., "Triboelectric Nanogenerator: A Foundation of the Energy for the New Era," Advanced Energy Materials, 9, pp. 25

[3] Wang L. Z., "On Maxwell's Displacement Current for Energy and Sensors: The Origin of Nanogenerators," 2017, Materials Today, 20, pp74-82, DOI 10.1016/j.mattod.2016.12.001.

[4] Jung W.-S., Kang M., Moon G. H., Baek S., Yoan S., Wang Z., Kim S., Kang C., "High Output Piezo/Triboelectric Hybrid Generator," 2015. Scientific Reports, 5, 9309, DOI 10.1038/srep09309.

[5] Xu L., Jiang T., Lin P., Shao J. J., He C., Zhong W., Chen Y. X., and Wang L. Z., 2018, "Coupled Triboelectric Nanogenerator Networks for Efficient Water Wave Energy Harvesting," ACS Nano, 12, pp.1849-1858.

[6] Xiu X., Xiangqian Z., Siyuan W., Han O., Pengfei C., Liguo S., Haichao Y., Yulong J., Peihong W., Zhou L., Minyi X., Zhong L. W., "Honeycomb Structure Inspired Triboelectric Nanogenerator for Highly Effective Vibration Energy Harvesting and Self-Powered Engine Condition Monitoring," 2019, Advanced Energy Materials, 9, doi 10.1002/aenm.201902460.

[7] Mann, K. 2019, "Triboelectric Generator for Energy Harvesting," M.S. Thesis, Mech. Eng. Dept, NPS, Monterey, CA.

THIS PAGE INTENTIONALLY LEFT BLANK

INITIAL DISTRIBUTION LIST

1. Defense Technical Information Center
   Ft. Belvoir, Virginia

2. Dudley Knox Library
   Naval Postgraduate School
   Monterey, California